Cerebral Cortex, March 2020;30: 1213–1233

doi: 10.1093/cercor/bhz161
Advance Access Publication Date: 5 August 2019
Original Article

ORIGINAL ARTICLE

Beyond the disconnectivity hypothesis of schizophrenia

Edmund T. Rolls[1,2,3,*,†], Wei Cheng[1,11,*,†], Matthieu Gilson[8], Weikang Gong[10], Gustavo Deco[8,9], Chun-Yi Zac Lo[1], Albert C. Yang[5], Shih-Jen Tsai[5], Mu-En Liu[5], Ching-Po Lin[1,4,6] and Jianfeng Feng[1,2,7,11,*]

[1]Institute of Science and Technology for Brain-inspired Intelligence, Fudan University, Shanghai, 200433, PR China, [2]Department of Computer Science, University of Warwick, Coventry CV4 7AL, UK, [3]Oxford Centre for Computational Neuroscience, Oxford OX1 4BH, UK, [4]Institute of Neuroscience, National Yang-Ming University, Taipei 11221, Taiwan, [5]Department of Psychiatry, Taipei Veterans General Hospital, Taipei 11267, Taiwan, [6]Brain Research Center, National Yang-Ming University, Taipei 11221, Taiwan, [7]School of Mathematical Sciences, School of Life Science and the Collaborative Innovation Center for Brain Science, Fudan University, Shanghai, 200433, PR China, [8]Center for Brain and Cognition, Computational Neuroscience Group, Department of Information and Communication Technologies, Universitat Pompeu Fabra, Roc Boronat 138, Barcelona E-08018, Spain and Brain and Cognition, Pompeu Fabra University, Barcelona, Spain, [9]Institució Catalana de la Recerca i Estudis Avançats (ICREA), Universitat Pompeu Fabra, Passeig Lluís Companys 23, Barcelona, 08010, Spain, [10]Centre for Functional MRI of the Brain (FMRIB), Nuffield Department of Clinical Neurosciences, Wellcome Centre for Integrative Neuroimaging, University of Oxford, Oxford, OX1 4BH, UK and [11]Key Laboratory of Computational Neuroscience and Brain-Inspired Intelligence (Fudan University), Ministry of Education, 200433, China

Address correspondence to Prof. Edmund T. Rolls, Department of Computer Science, University of Warwick, Coventry CV4 7AL, UK. Email: Edmund.Rolls@oxcns.org, www.oxcns.org; Dr. Wei Cheng, Institute of Science and Technology for Brain-inspired Intelligence, Fudan University, Shanghai 200433, China. Tel.: 86-21-55665593, Email: wcheng.fdu@gmail.com; Prof. Jianfeng Feng, Institute of Science and Technology for Brain-inspired Intelligence, School of Mathematical Sciences, Fudan University, Shanghai 200433, China, and Department of Computer Science, University of Warwick, Coventry CV4 7AL, UK. Tel.: 86-21-65643621, Email: jianfeng64@gmail.com. https://orcid.org/0000-0003-3025-1292
[†]These authors contributed equally to this work.

Abstract

To go beyond the disconnectivity hypothesis of schizophrenia, directed (effective) connectivity was measured between 94 brain regions, to provide evidence on the source of the changes in schizophrenia and a mechanistic model. Effective connectivity (EC) was measured in 180 participants with schizophrenia and 208 controls. For the significantly different effective connectivities in schizophrenia, on average the forward (stronger) effective connectivities were smaller, whereas the backward connectivities tended to be larger. Further, higher EC in schizophrenia was found from the precuneus and posterior cingulate cortex (PCC) to areas such as the parahippocampal, hippocampal, temporal, fusiform, and occipital cortices. These are backward effective connectivities and were positively correlated with the positive symptoms of schizophrenia. Lower effective connectivities were found from temporal and other regions and were negatively correlated with the symptoms, especially the negative and general symptoms. Further, a signal variance parameter was increased for areas that included the parahippocampal gyrus and hippocampus, consistent with the hypothesis that hippocampal overactivity is involved in schizophrenia. This investigation goes beyond the disconnectivity hypothesis by drawing

attention to differences in schizophrenia between backprojections and forward connections, with the backward connections from the precuneus and PCC implicated in memory stronger in schizophrenia.

Key words: effective connectivity, medial prefrontal cortex, orbitofrontal cortex, precuneus, posterior cingulate cortex, schizophrenia

Introduction

Schizophrenia is a disorder often characterized by positive, cognitive, and negative symptoms (Mueser and McGurk 2004), which may have different neurobiological bases (Rolls et al. 2008; Rolls 2012a). The positive (psychotic or thought disorder) symptoms may include hallucinations, delusions, and paranoia. The cognitive symptoms may include a failure to maintain attention, and deficits in short-term memory that is required to maintain attention. The negative symptoms may include reduced emotion and motivation, including reduced hedonia. It has been shown that the major difference between patients is in the negative symptoms (Rolls et al. 2017), measured with the positive and negative syndrome scale (PANSS) (Kay et al. 1987).

The etiology and neuropathophysiological mechanism of this debilitating and severe disorder remain unclear. Evidence for structural and functional deficits in the brain of schizophrenia has been developed into a disconnectivity hypothesis (Friston and Frith 1995). More direct evidence for the disconnectivity hypothesis comes mainly from functional magnetic resonance imaging (fMRI) studies, particularly resting-state fMRI studies, which have shown widespread functional disconnectivity in distributed brain networks in schizophrenia (Khamsi 2012; Smith 2012; Friston et al. 2016; Northoff and Duncan 2016). However, very consistent patterns and principles of altered connectivity in schizophrenia remain somewhat elusive (Meyer-Lindenberg 2010; Whitfield-Gabrieli and Ford 2012; Northoff and Duncan 2016). In one study, first-episode patients had many differences in functional connectivity (FC) involving the inferior frontal gyri (Broca's area), and these changes were correlated with delusion / blunted affect (Li et al. 2017).

Resting state FC, which reflects correlations in the activity between brain areas, is widely used to help understand human brain function in health and disease (Deco and Kringelbach 2014; Cheng et al. 2016). Here we go beyond FC to effective connectivity (EC) between different brain areas to measure directed influences of human brain regions on each other. EC is conceptually very different, for it measures the effect of one brain region on another in a particular direction, and can in principle therefore provide information more closely related to the causal processes that operate in brain function, that is, how one brain region influences another. In the context of disorders of brain function, the EC may provide evidence on which brain regions may have altered function, and then influence other brain regions, by comparing EC in patients and control participants.

In this paper we utilize a new approach to the measurement of EC in which each brain area has a simple dynamical model, and known anatomical connectivity is used to provide constraints (Gilson et al. 2016; Gilson et al. 2018; Rolls et al. 2018). This helps the approach to measure the EC between the 94 automated anatomical atlas (AAL2) (Rolls et al. 2015) brain areas using resting-state fMRI. (The names of the AAL2 areas are shown in Supplementary Table S1, and the areas can be viewed with the Mricron viewer.) Moreover, we show how the approach can be used to measure the differences in EC between different groups of individuals, using as an example EC in the healthy brain and in individuals with schizophrenia. This results in the first brain-wide resting state effective-connectivity neuroimaging analysis of schizophrenia.

Materials and Methods

Participants

There were 180 patients with a diagnosis of schizophrenia, and 208 healthy controls. The patients were from Taiwan (Veteran General Hospital, Taipei), and the Center for Biomedical Research Excellence (COBRE, http://fcon_1000.projects.nitrc.org/indi/retro/cobre.html) (Mayer et al. 2013; Cheng et al. 2015a). All patients were diagnosed according to the DSM-IV diagnostic criteria by qualified psychiatrists using a best estimate procedure that utilized all available clinical information including a diagnostic interview, clinical case notes, the clinician's observations, and informant reports. Symptom severity was measured using the PANSS assessment (Kay *et al.* 1987) given to all patients either one week before the MRI scan or one week after it. All patients were medicated. Table S2 provides a summary of the demographic information and the psychiatric diagnosis of the participants, and fuller information is provided in the Supplementary material.

Data acquisition and preprocessing

All the Taiwan and COBRE imaging data were acquired using a 3-T Siemens Trio Tim MRI scanner with an 8- or a 12- channel phased array head coil. Participants were instructed to relax, hold still, keep their eyes closed, and think of nothing in particular. The Supplementary material provides additional details of the imaging acquisition.

Resting-state fMRI data were preprocessed using FMRIB Software Library (FSL) (Jenkinson et al. 2012) and Analysis of Functional NeuroImages (AFNI) (Cox 1996). For each individual, the preprocessing steps included slice-timing correction (FSL slicetimer), motion correction (FSL mcflirt), spatial smoothing by a 3D Gaussian kernel (FWHM = 6 mm), despiking motion artifacts using the Brain-Wavelet Toolbox (Patel et al. 2014), registering to a $3 \times 3 \times 3$ mm^3 standard space by first aligning the functional image to individual T1 structural images using boundary based registration (Greve and Fischl 2009) and then to standard space using FSL's linear and non-linear registration tool (FSL flirt and fnirt), white matter signal, cerebrospinal fluid signal. The global signal was not regressed out for reasons provided by (Cheng *et al.* 2016). Care was taken to avoid any effects of head motion by regressing out nuisance covariates including Friston's 24-head motion parameters, and by excluding data from participants with any head motion >0.5 mm. In addition, mean head motion was regressed out of all analyses. Further, no significant differences in head motion were found between the patients and controls. No temporal filtering was used (in order to provide the best time resolution for the EC, but the linear changes in the blood oxygenation-level dependent (BOLD) signal time series were regressed out to remove any linear trends in the data).

We checked and confirmed that the main results shown in this paper, for example, the difference between the connectivity in the forward and backward directions in schizophrenia described below, were not found only with this filtering, for very similar results were obtained when the full dataset was re-preprocessed with the high pass temporal filtering set to the more usual 0.01 Hz, so that the temporal filter was 0.01–max Hz, as shown in the Supplementary material. All the images were manually checked to ensure successful preprocessing. The resulting time courses were used for the construction and analysis of the brain network.

After preprocessing, the whole brain (gray matter) was parcellated into 94 anatomically defined regions using the automated anatomical labeling atlas (AAL2; Rolls *et al.* 2015) that includes a useful parcellation of the orbitofrontal cortex. The time series were extracted in each region by averaging the signals of all voxels within that region. The names of the regions are provided in Supplementary Table S1.

EC measurement

Introduction

A classical approach to measuring EC is dynamic causal modeling (DCM) (Friston 2009; Valdes-Sosa et al. 2011; Bajaj et al. 2016). DCM is often used with circuits consisting of a priori selected brain regions to test hypotheses on the interactions between the considered regions. Here we instead use a network model with simpler assumptions than those typically used in DCM to perform a large-scale connectivity analysis involving many brain areas (Gilson *et al.* 2016). This allows for the very efficient calculation of maximum-likelihood EC estimates for a large number (94) of nodes, individually for a large cohort of participants. In this way we target significant EC differences for all existing connections (as determined by diffusion tensor imaging [DTI]) that characterize schizophrenia with FDR correction and without preliminary knowledge, expecting a distributed pattern of abnormal EC links across the brain. Our estimation procedure (Gilson *et al.* 2016) iteratively optimizes a network model such that it reproduces the empirical cross-covariances between ROIs, which are canonically related to the cross-spectral density used in recent studies that apply DCM to resting-state fMRI data (Friston et al. 2014; Razi et al. 2017). The model uses an exponential approximation of BOLD autocovariance (locally over a few TRs) and discards very slow-frequency fluctuations. Moreover, by using data without temporal filtering, we were able to dispense with a model of haemodynamic mapping neuronal activity to fMRI signals, as the corresponding time constants are faster (Friston 2002). Finally, we place positivity constraints on extrinsic or between node connections—in line with known neuroanatomy and previous modeling studies (Marreiros et al. 2008). A last simplification compared to DCM includes a fixed (but plausible) form of endogenous neuronal fluctuations (Σ in our model) that were characterized by a single (variance) parameter in each region or node. In spite of these differences, we still borrow the term "effective connectivity" from the DCM literature as our connectivity estimates relate to directional interactions between ROIs in the brain network. This model-based approach has been successfully applied to identify changes in the cortical coordination between rest and movie viewing (Gilson *et al.* 2018), and to EC in depression (Rolls *et al.* 2018).

Compared to DCM the new method used here (Gilson *et al.* 2016) is computationally more efficient and thus can analyze larger networks because it limits the degrees of freedom for each brain region by utilizing a simpler model of each brain region, and because it uses some structural connectivity information from, for example, DTI. Further, the new EC method focuses on transitions between fMRI "activity states" across successive time points (Mitra et al. 2015) and does not include details about hemodynamics like the Balloon model (Friston et al. 2000). The estimated EC measures the strengths of causal interactions from one brain area to another, via the proxy of BOLD fluctuations; it provides a single number that lumps together the effects of the strength of the synapse, and neurotransmitter release, etc. The synaptic conductivity interpretation also relates to our earlier neuron-level models in which the synaptic conductivity between modules is a key parameter that specifies how much one module influences another module (Rolls et al. 2012). The new method has the additional advantage that each brain region or module has its own Σ parameter that specifies the variance of the module's activity, which may be related to the intrinsic excitability of the region. In relation to our integrate-and-fire models, the parameter $w+$ that defines the strength of the recurrent collateral synapses within the attractor network (Rolls *et al.* 2012) may relate to the Σ parameter in the current EC approach (Gilson *et al.* 2016), because the local feedback influenced by $w+$ influences the fluctuations of the activity, for example, how readily an area will transition to a high-firing rate state. That is, Sigma corresponds in the model to the spontaneous activity (its variance) of a region, and this propagates via the effective connectivities to the other nodes in the recurrent network. A higher value for Sigma compared relative to controls indicates more fluctuating activity, which could reflect a pathological increase of activity.

The EC model and algorithm used here is closely related to the linearized version of the DCM that is used for the resting state (Friston *et al.* 2014; Frassle et al. 2017) and for task-related fMRI (Gilson *et al.* 2018). Although the hemodynamics of the filtering is properly modeled for DCM, the complex nonlinearity is simplified in the EC algorithm used here (Gilson *et al.* 2016), which enables it to be applied to a whole-brain parcellation with many nodes (in this case, the 94 nodes of the AAL2 atlas). Instead of the model comparison used by DCM to find the best network topology, the current algorithm uses structural data (from DTI) to specify possible connections in the model, thereby simplifying the operation of the model because some links with no known anatomical connection are excluded. The implication is that significant differences of EC identified with this algorithm (here schizophrenia vs. controls) are expected to reflect significant changes in the corresponding DCM.

Within a cortical hierarchy of connectivity (e.g., from primary visual cortex V1 to the inferior temporal cortex; Rolls 2012b), the forward connections between any pair of cortical areas up through the hierarchy are thought to be stronger than the backprojections based on a wealth of evidence (Rolls 2016a), and there are useful asymmetries in the terminations of the forward and backward projections that facilitate this (Pandya et al. 2015; Rolls 2016a). This ensures that sensory input dominates the processing, rather than imagination. In the present investigation, we refer to the EC in terms of how region 1 influences region 2, and refer to forward and backward connectivity mainly in the Discussion. The EC algorithm used here was validated by the forward versus backward connectivities in the healthy controls. For example, the EC was greater from the inferior temporal cortex to the medial orbitofrontal cortex (0.04 vs. 0.03), which is predicted to be forward connectivity (Rolls 2016a, 2019). In another example, the EC was greater from the inferior temporal

cortex to the parahippocampal gyrus (0.04 vs. 0.02), which is predicted to be forward connectivity (Rolls 2016a). In another example, the EC was greater from the inferior temporal cortex to the hippocampus (0.03 vs. 0.02), which is predicted to be forward connectivity (Rolls 2016a). Further examples can be seen in the whole Table of effective connectivities between all 94 AAL2 area in a different group of healthy participants available elsewhere (Rolls *et al.* 2018).

Overview

The approach used to calculate EC follows that described by Gilson et al. (2016). EC measures the individual efficacy of each existing connection between two brain regions, that is, how much one brain region influences another. Our approach provides a signature for each subject in the high-dimensional space of EC connections (>3000), which is then used to investigate differences between schizophrenia patients and healthy controls. The estimated EC values reflect the combined effects of synaptic efficacies between the regions, the types and concentrations of neurotransmitters in the target regions, etc.

The dynamics for each brain region are described by a multivariate Ornstein–Uhlenbeck process; each region receives fluctuating inputs (white noise) that propagates via the EC to other nodes, which shapes the correlation pattern at the global level, that is, the FC. Here the focus is on transitions of fMRI measurements across successive TRs, which have been shown to convey information about conditions such as waking versus sleeping (Mitra *et al.* 2015). The EC model captures this information via the covariances with non-zero time shifts (spatiotemporal FC) and the resulting EC contains information about directed connectivity. Both EC and the local input variance are optimized such that the model best reproduces statistics of observed fMRI signals measured by the empirical spatiotemporal FC, which are canonically related to the cross spectra used to tune a resting-state DCM (Friston *et al.* 2014).

Details about the optimization are provided by Gilson et al. (2016) for resting-state fMRI data and are summarized next. The skeleton for the EC is provided by structural data obtained using DTI, from which we infer the existence of connections. This usefully reduces the number of parameters to estimate and enhances the estimation procedure at the level of individual subjects: from all possible $94^2 - 94 = 8742$ connections, we specify that many are not present anatomically as direct projections, so in the model we need to optimize only 39% of the possible connections. The DTI connectivity matrix was set to just 0 (no connection) or 1 (for a connection) between the AAL2 94 regions (Rolls *et al.* 2015), based on the DTI atlas used by Gilson et al. (2016). The algorithm thus limits the number of parameters being considered, by excluding connections in the model for which there is no anatomical basis for a direct connection between brain areas, and uses the structural connectivity in this way. A key advantage of the approach is that it does not have to limit the number of nodes considered in the EC model by any prior hypothesis involving selecting only some nodes for analysis, except those with no known direct anatomical connection. Because DTI may miss inter-hemispheric connections between homotopic regions between the two hemispheres (Hagmann et al. 2008; Messe et al. 2014), we set these as being present, and allowed the algorithm to tune the strengths of these just as for the other effective connectivities. In the present investigation the 1's in the connectivity matrix were the same as those established for the human brain and used previously (Gilson *et al.* 2016). The AAL2 (Rolls *et al.* 2015) was used to parcellate the brain into 94 regions, because this number of regions provides a suitable number of FC links without too many degrees of freedom; because its parcellation of the orbitofrontal cortex region which is of special interest in relation to depression (Rolls 2016b) has been remade to relate to useful divisions and descriptions; and because it has been found to be useful in related investigations (Cheng *et al.* 2016). Limiting the number of parameters to estimate in the whole-brain dynamic model is crucial to obtain robust individualized EC estimates. On the other hand, the AAL2 corresponds to about 3450 EC link parameters (for 39.46% density), which is a sufficiently rich space to extract complex patterns to differentiate between patients and controls. Our choice aimed to solve this trade-off. We note that this approach to the estimation of EC is being widely used (Gilson 2018; Gilson et al. 2018; Pallares et al. 2018; Rolls et al. 2018; Senden et al. 2018).

Empirical covariances:

For the resting-state session of each individual, we denote the centered (zero-mean) time series by s_i^t for region $1 \le i \le N$ with time $1 \le t \le T$; the duration is $T = 190$ for the Taiwan dataset and $T = 150$ for the COBRE dataset. The zero-lag and 1-lag covariances are calculated as follows:

$$\hat{Q}_{ij}^0 = \frac{1}{T-2}\sum\nolimits_{1\le t\le T-1} s_i^t s_j^t \quad \text{and} \quad \hat{Q}_{ij}^1 = \frac{1}{T-2}\sum\nolimits_{1\le t\le T-1} s_i^t s_j^{t+1} \qquad (1)$$

For each subject, we evaluate the time constant τ_x associated with the exponential decay of the autocovariance function $\hat{Q}_{ii}^{\tau}$ averaged over all regions:

$$\tau_x = \frac{N}{\sum_i \log\left(\hat{Q}_{ii}^0\right) - \log\left(\hat{Q}_{ii}^1\right)}. \qquad (2)$$

Dynamic cortical model:

The model comprised $N = 94$ interconnected cortical regions. The activity x_i of each region is governed by an Ornstein–Uhlenbeck process and evolves depending on the activity of other populations: $\frac{dx_i}{dt} = \frac{-x_i}{\tau_x} + \sum_{j\ne i} C_{ij} x_j + dB_i$. Here, the time constant τ_x corresponds to an exponential decay and is calibrated from the empirical data (see Eq. 2); dB_i is white Gaussian noise with covariance matrix Σ, where the input variances sit on the diagonal and are zero elsewhere. These input fluctuations propagate via the EC embodied by the matrix C (its skeleton is determined by DTI). All variables x_i have zero mean and the theoretical spatiotemporal covariances are defined by $Q_{ij}^{\tau} = \left\langle x_i^t x_j^{t+\tau} \right\rangle$, where the angular brackets denote averaging over randomness of the inputs; we use two time shifts: $\tau = 0$ and $\tau = 1$ TR.

The mathematical mappings between matrices C, Q^0, and Q^1 are given by Lyapunov equation $JQ^0 + Q^0 J^T + \Sigma = 0$ and $Q^1 = Q^0 \mathrm{expm}(J^T)$, where the Jacobian of the dynamical system $J_{ij} = -\frac{\delta_{ij}}{\tau_x} + C_{ij}$ depends on the mean activity of the network (δ_{ij} is the Kronecker delta); the superscript T denotes the matrix transpose; expm denotes the matrix exponential. These two consistency equations allow for the quick estimation of the predicted FC matrices, without simulating the network.

In the current form of the EC algorithm, there is no hemodynamic model (Gilson *et al.* 2016), but any possible difference in the hemodynamics between schizophrenics and controls is unlikely to account for the results described here, in that it is

very unlikely, for example, that this could lead to the decrease in the forward connectivity and the increase in the backward connectivity for the links that are significantly different between schizophrenics and controls. Further, Figure 3A shows that in people with schizophrenia, across the whole brain the weaker EC links tend to be increased in strength relative to controls, and the strong EC links tend to be decreased in strength relative to controls ($r = 0.39$, $P < 0.0001$), and it is unlikely that any difference in haemodynamic responses between schizophrenics and controls would account for exactly these effects shown in Figure 3A. However, we note that it would nevertheless be of interest in future research to investigate possible differences in the haemodynamics between people with schizophrenia and controls, even though this is unlikely given the above arguments to be able to account for all the differences in the forward versus backward connectivity of almost all of the EC links described here that are significantly different in schizophrenia. Further information about the mathematical model is provided in the Supplementary material in the Section 'The dynamic cortical model for EC'.

Parameter estimation procedure:
We tune the model such that its covariance matrices Q^0 and Q^1 reproduce the empirical $\hat{Q}^0$ and $\hat{Q}^1$. We summarize the essential steps of the procedure described in Gilson et al. (2016) that iteratively optimizes the network parameters C and Σ. At each step, the Jacobian J is calculated from the current value of C. Then, the model FC matrices Q^0 and Q^τ are calculated from the consistency equations, using the Bartels–Stewart algorithm to solve the Lyapunov equation. The desired Jacobian update is the matrix $\delta J^T = (Q^0)^{-1}\left[\delta Q^0 + \delta Q^1 \exp(-J^T)\right]$, which aims to reduce the FC error between the empirical and model FC, as determined by the two difference matrices $\delta Q^0 = \hat{Q}^0 - Q^0$ and $\delta Q^1 = \hat{Q}^1 - Q^1$. Finally, the connectivity update is $\delta C_{ij} = \eta_C \delta J_{ij}$ for existing connections. We impose non-negativity of the EC values during the optimization. The input variances are tuned according to $\delta \Sigma_{ii} = -\eta_\Sigma \left(J \delta Q^0_{ii} + \delta Q^0_{ii} J^T\right)$. We use $\eta_C = 0.0001$ and $\eta_\Sigma = 0.1$.

The approach has been shown to be robust, in that it has been shown that the EC measured in this way conveys relevant information about subject and (task) conditions, thereby making EC a useful connectivity measure for biomarkers (Pallares *et al.* 2018). EC measured with this algorithm was found to be more robust than FC in an analysis of this issue (Pallares *et al.* 2018). The choice of η_C and η_Σ is in line with a previous study that explored the estimation of EC (Gilson *et al.* 2016). They are also in a similar range to those used for biomarkers (Pallares *et al.* 2018).

The EC algorithm produces values for the EC between every pair of nodes (apart from those set to zero by the anatomical mask) in the AAL2 atlas, and every connection in the resulting EC matrix is a direct connection. For clarification, the optimization method that tunes the EC weights takes into account the network effects (Gilson *et al.* 2016). This means that the observed correlations (FC0 and FC1) are generated by the EC weights while incorporating indirect interactions. In essence this is like partial correlations compared to Pearson correlations for a graphical model, the former often being a sparse matrix even when the second is a full matrix. Of course, it is possible that any one node in the model may have internal connections in addition to those being measured by the algorithm, with one example being the hippocampus which has dentate to CA3 to CA1 internal connectivity (Rolls 2018). The algorithm deals with the interaction of the specified nodes, and not of all the internal interactions between the neurons within each node. But the EC algorithm (Gilson *et al.* 2016) itself does measure direct effects between the nodes in the model, which in the present research are the 94 brain areas in the automated anatomical labeling atlas AAL2 (Rolls *et al.* 2015).

In addition, the EC algorithm does allow negative effectivity connectivities to be calculated, which might reflect, for example, inhibition from one area to another, but when this was checked, any negative EC values in the AAL2 matrix were few and small in magnitude, with only one exceeding a threshold of −0.03, and only 35/3450 link parameters between −0.01 and −0.03. In further checks, it was found that the correlation between the EC values with the standard clipping of effective connectivities at zero and allowing them to become negative was high ($r = 0.99$, across the whole group and for all links), so that the conclusions reached in this paper are very little affected by whether the links are clipped at zero or not. Further, the finding reported in the results below that the difference between the forward and backward effective connectivities was lower in schizophrenia was confirmed also when the algorithm was allowed to run with effective connectivities that could assume negative values. For example, the difference between the forward and backward effective connectivities was considerably smaller in the schizophrenia group than in the controls ($t = 3.77$, $P = 1.86e\text{-}4$) with the clipping at zero as shown below. This finding was confirmed when there was no clipping of effective connectivities at zero ($t = 4.86$, $P = 1.7e\text{-}6$).

The goodness of the fit of the model used to generate the EC to the empirical data was assessed as follows. The correlation between the FC produced by the EC model and the empirical FC measured between all AAL2 areas was 0.67 (with 0.08 standard error), which provided evidence of a satisfactory operation of the model, in line with what was reported by Gilson et al. (2016).

Normalization of model estimates:
Normalization of the EC within each individual was performed by performing the z-score over the matrix elements for each EC matrix within each participant: (EC_{ij} – mean (EC_{ij}))/std (EC_{ij}) for all EC links (performed over existing links corresponding to 1's in the structural connectivity matrix). The aim of this was to enable each participant's data to contribute similarly to the statistics calculated across participants. We note that small effective connectivities will appear in the tables in this paper as negative, but this is only due to the removal of the mean value. All EC links computed by the algorithm are in fact positive. Any difference between patients and controls that is described as negative in fact refers only to a decrease of EC. A similar normalization within each individual was used for the Σ values. An increase of a Σ value can be interpreted as an increase of the variance in an AAL2 region. These normalisations were used for the statistical calculations. Table 1 shows the mean of the EC values not normalized (because a negative EC would have no meaning). Table 2 shows the mean of the Σ values normalized within each participant because this better reflects the statistical values.

Statistical analysis of EC
Two-tailed, two-sample *t*-tests were performed on the normalized EC to identify significantly altered EC links in patients compared to controls within each imaging center that provided resting-state fMRI data. The effects of age, gender ratios, head motion, and education were regressed within each dataset

Table 1 EC links that are different between patients with schizophrenia and controls

Region 1 (R1)	Region 2 (R2)	t value of R1 to R2	P value of R1 to R2	EC of R1 to R2 in CON	EC of R1 to R2 in SCZ	t value of R2 to R1	P value of R2 to R1	EC of R2 to R1 in CON	EC of R2 to R1 in SCZ	F/B ratio in CON	F/B ratio in SCZ
Amygdala_L	Postcentral_L	−5.2193	1.80E-07	0.0263	0.0188	0.2086	8.35E-01	0.0315	0.0338	1.1958	1.8022
Amygdala_L	Insula_L	−4.4472	8.70E-06	0.0184	0.0135	0.2348	8.14E-01	0.0383	0.0470	2.0809	3.4830
Frontal_Sup_2_L	Supp_Motor_Area_L	4.6475	3.36E-06	0.0403	0.0601	1.8255	6.79E-02	0.0295	0.0359	1.3658	1.6750
Fusiform_L	Lingual_L	−5.3568	8.47E-08	0.0899	0.0819	0.6311	5.28E-01	0.0418	0.0473	2.1479	1.7318
Fusiform_L	Lingual_R	−4.4415	8.94E-06	0.0771	0.0722	0.7594	4.48E-01	0.0301	0.0342	2.5635	2.1106
Fusiform_L	Cuneus_R	−4.4318	9.35E-06	0.0579	0.0514	0.8655	3.87E-01	0.0174	0.0203	3.3292	2.5390
Fusiform_L	Occipital_Sup_L	−4.2990	1.72E-05	0.0623	0.0543	1.1122	2.66E-01	0.0222	0.0255	2.8040	2.1239
Heschl_L	Temporal_Mid_L	−5.3753	7.65E-08	0.0194	0.0138	−2.5027	1.23E-02	0.0325	0.0268	1.6761	1.9488
Heschl_L	Cingulate_Mid_L	−4.7948	1.63E-06	0.0377	0.0302	−1.8460	6.49E-02	0.0389	0.0370	1.0322	1.2246
Heschl_L	Temporal_Sup_L	−4.6520	3.29E-06	0.0582	0.0524	−0.0540	9.57E-01	0.0751	0.0781	1.2904	1.4917
Heschl_L	Heschl_R	−4.3079	1.65E-05	0.0733	0.0659	−1.2915	1.97E-01	0.0699	0.0686	1.0493	0.9603
Heschl_L	Precentral_L	−4.2601	2.04E-05	0.0221	0.0177	−4.4511	8.54E-06	0.0513	0.0424	2.3164	2.3977
Heschl_R	Temporal_Pole_Sup_R	−4.5764	4.73E-06	0.0346	0.0306	−3.3522	8.02E-04	0.0532	0.0489	1.5406	1.5953
Pallidum_L	Thalamus_L	−5.1315	2.87E-07	0.0497	0.0411	0.2162	8.29E-01	0.0308	0.0342	1.6151	1.2025
Pallidum_R	Thalamus_R	−5.0929	3.53E-07	0.0424	0.0347	−1.9382	5.26E-02	0.0313	0.0308	1.3545	1.1262
Pallidum_R	Thalamus_L	−4.6029	4.17E-06	0.0421	0.0348	−0.6891	4.91E-01	0.0269	0.0275	1.5666	1.2640
Pallidum_R	Frontal_Inf_Oper_R	−4.5095	6.50E-06	0.0382	0.0312	−1.7284	8.39E-02	0.0226	0.0209	1.6929	1.4934
Paracentral_Lobule_L	Postcentral_L	−6.6846	2.32E-11	0.0541	0.0413	1.1861	2.36E-01	0.0733	0.0871	1.3559	2.1072
Paracentral_Lobule_L	Postcentral_R	−6.2891	3.19E-10	0.0513	0.0415	0.7514	4.52E-01	0.0638	0.0768	1.2451	1.8488
Paracentral_Lobule_L	Precentral_R	−5.6940	1.24E-08	0.0472	0.0368	0.0314	9.75E-01	0.0847	0.0979	1.7939	2.6569
Paracentral_Lobule_L	Occipital_Sup_L	−4.8917	1.00E-06	0.0396	0.0301	1.6293	1.03E-01	0.0262	0.0351	1.5128	0.8578
Paracentral_Lobule_L	Precentral_L	−4.3740	1.22E-05	0.0358	0.0293	−1.6939	9.03E-02	0.0775	0.0836	2.1627	2.8543
Paracentral_Lobule_R	Postcentral_L	−4.9811	6.32E-07	0.0450	0.0355	0.7350	4.62E-01	0.0672	0.0798	1.4943	2.2521
Paracentral_Lobule_R	Postcentral_R	−4.8783	1.07E-06	0.0498	0.0421	1.4725	1.41E-01	0.0701	0.0854	1.4086	2.0267
Paracentral_Lobule_R	Precentral_R	−4.7478	2.06E-06	0.0420	0.0333	−0.4239	6.72E-01	0.0842	0.0941	2.0051	2.8290
ParaHippocampal_L	Occipital_Sup_L	−5.0958	3.47E-07	0.0317	0.0204	1.4964	1.35E-01	0.0087	0.0101	3.6303	2.0178
ParaHippocampal_L	Occipital_Mid_L	−4.8364	1.32E-06	0.0365	0.0284	2.2489	2.45E-02	0.0176	0.0255	2.0792	1.1162
ParaHippocampal_L	Lingual_L	−4.6352	3.57E-06	0.0482	0.0365	−0.4049	6.86E-01	0.0161	0.0165	2.9964	2.2064
ParaHippocampal_R	Lingual_R	−6.1206	9.32E-10	0.0671	0.0493	0.9885	3.23E-01	0.0141	0.0161	4.7627	3.0576
ParaHippocampal_R	Calcarine_R	−5.8300	5.54E-09	0.0642	0.0455	2.3091	2.09E-02	0.0145	0.0181	4.4251	2.5134
ParaHippocampal_R	Temporal_Pole_Sup_R	−5.8127	6.15E-09	0.0533	0.0412	−0.7388	4.60E-01	0.0292	0.0295	1.8276	1.3958
ParaHippocampal_R	Occipital_Mid_R	−5.8126	6.15E-09	0.0606	0.0472	−0.3197	7.49E-01	0.0203	0.0223	2.9769	2.1175
ParaHippocampal_R	Cuneus_R	−5.7365	9.67E-09	0.0537	0.0373	1.3852	1.66E-01	0.0089	0.0106	6.0032	3.5131
ParaHippocampal_R	Occipital_Sup_R	−5.0802	3.77E-07	0.0428	0.0318	−1.0477	2.95E-01	0.0115	0.0105	3.7183	3.0431
ParaHippocampal_R	Insula_R	−4.2807	1.86E-05	0.0340	0.0219	0.3900	6.97E-01	0.0135	0.0158	2.5126	1.3889
Postcentral_R	Lingual_R	−4.2540	2.10E-05	0.0452	0.0376	−2.9510	3.17E-03	0.0233	0.0200	1.9413	1.8838
Precentral_L	Postcentral_L	−4.7826	1.73E-06	0.0897	0.0822	2.4831	1.30E-02	0.0569	0.0688	1.5752	1.1952
Precentral_L	Supp_Motor_Area_L	4.5363	5.73E-06	0.0726	0.0942	−2.3719	1.77E-02	0.0452	0.0450	1.6058	2.0930
Precentral_L	Heschl_L	−4.4511	8.54E-06	0.0513	0.0424	−4.2601	2.04E-05	0.0221	0.0177	2.3164	2.3977
Precuneus_L	Fusiform_L	5.3789	7.49E-08	0.0023	0.0054	3.1195	1.81E-03	0.0396	0.0525	17.0610	9.6510
Precuneus_L	ParaHippocampal_L	5.0288	4.94E-07	0.0068	0.0125	−1.8669	6.19E-02	0.0605	0.0568	8.9613	4.5589

(Continued)

Table 1 Continued

Region 1 (R1)	Region 2 (R2)	t value of R1 to R2	P value of R1 to R2	EC of R1 to R2 in CON	EC of R1 to R2 in SCZ	t value of R2 to R1	P value of R2 to R1	EC of R2 to R1 in CON	EC of R2 to R1 in SCZ	F/B ratio in CON	F/B ratio in SCZ
Precuneus_L	Parietal_Sup_L	4.7247	2.30E-06	0.0254	0.0402	1.1738	2.40E-01	0.0521	0.0634	2.0464	1.5770
Precuneus_L	Fusiform_R	4.2981	1.72E-05	0.0021	0.0042	3.3588	7.83E-04	0.0302	0.0423	14.3434	10.1715
Precuneus_R	ParaHippocampal_L	5.4387	5.37E-08	0.0069	0.0141	−1.7725	7.63E-02	0.0550	0.0538	7.9936	3.8070
Precuneus_R	Fusiform_L	5.0988	3.42E-07	0.0032	0.0070	2.5356	1.12E-02	0.0390	0.0500	12.0392	7.0871
Precuneus_R	ParaHippocampal_R	4.7037	2.56E-06	0.0074	0.0127	−1.9131	5.57E-02	0.0740	0.0720	9.9728	5.6650
Precuneus_R	Occipital_Mid_R	4.5290	5.93E-06	0.0074	0.0156	3.1990	1.38E-03	0.0333	0.0495	4.5179	3.1816
Precuneus_R	Parietal_Sup_L	4.4302	9.42E-06	0.0196	0.0338	1.3378	1.81E-01	0.0398	0.0503	2.0255	1.4908
Putamen_R	Frontal_Inf_Oper_R	−5.1022	3.36E-07	0.0445	0.0373	−2.4688	1.36E-02	0.0261	0.0240	1.7066	1.5528
Putamen_R	SupraMarginal_R	−4.3114	1.62E-05	0.0515	0.0438	−2.8078	4.99E-03	0.0206	0.0164	2.4960	2.6648
Rolandic_Oper_L	Fusiform_L	−4.3516	1.35E-05	0.0302	0.0254	−2.6644	7.71E-03	0.0367	0.0322	1.2174	1.2678
Supp_Motor_Area_L	Rolandic_Oper_L	−5.6160	1.95E-08	0.0368	0.0264	−2.8934	3.81E-03	0.0381	0.0362	1.0345	1.3688
Supp_Motor_Area_L	Insula_L	−4.5579	5.17E-06	0.0341	0.0274	−0.3866	6.99E-01	0.0443	0.0460	1.2991	1.6803
Supp_Motor_Area_L	Precentral_R	−4.3974	1.10E-05	0.0423	0.0372	4.0272	5.65E-05	0.0658	0.0860	1.5563	2.3131
Supp_Motor_Area_R	Precentral_R	−5.6360	1.74E-08	0.0629	0.0544	3.1723	1.51E-03	0.0620	0.0764	1.0157	0.7125
Supp_Motor_Area_R	Insula_R	−5.5575	2.74E-08	0.0531	0.0435	−0.8708	3.84E-01	0.0309	0.0303	1.7195	1.4360
Supp_Motor_Area_R	Rolandic_Oper_R	−5.0939	3.51E-07	0.0619	0.0543	−0.3774	7.06E-01	0.0319	0.0354	1.9388	1.5333
Supp_Motor_Area_R	Postcentral_L	−4.7120	2.45E-06	0.0509	0.0434	3.7217	1.98E-04	0.0372	0.0487	1.3703	0.8900
Supp_Motor_Area_R	Putamen_R	−4.5465	5.45E-06	0.0251	0.0181	−2.9881	2.81E-03	0.0319	0.0297	1.2721	1.6419
Supp_Motor_Area_R	Frontal_Inf_Oper_R	−4.2597	2.05E-05	0.0512	0.0447	−2.4420	1.46E-02	0.0396	0.0407	1.2930	1.0976
Temporal_Mid_L	Cuneus_R	−4.4098	1.03E-05	0.0304	0.0218	−0.1722	8.63E-01	0.0111	0.0117	2.7507	1.8676
Temporal_Pole_Mid_L	Temporal_Sup_L	−5.6735	1.40E-08	0.0391	0.0263	−2.4005	1.64E-02	0.0200	0.0175	1.9574	1.4983
Temporal_Pole_Mid_L	Occipital_Mid_L	−5.6373	1.73E-08	0.0303	0.0202	0.5535	5.80E-01	0.0094	0.0113	3.2127	1.7809
Temporal_Pole_Mid_L	Occipital_Inf_L	−4.9666	6.82E-07	0.0436	0.0324	0.9313	3.52E-01	0.0095	0.0102	4.5905	3.1892
Temporal_Pole_Mid_L	Fusiform_L	−4.6470	3.37E-06	0.0409	0.0354	0.8199	4.12E-01	0.0278	0.0335	1.4710	1.0554
Temporal_Pole_Mid_L	Calcarine_L	−4.4301	9.42E-06	0.0420	0.0316	2.4475	1.44E-02	0.0067	0.0094	6.2522	3.3733
Temporal_Pole_Mid_L	Lingual_L	−4.3218	1.55E-05	0.0399	0.0294	0.1528	8.79E-01	0.0110	0.0111	3.6268	2.6606
Temporal_Pole_Mid_L	Temporal_Pole_Sup_L	−4.2944	1.75E-05	0.0856	0.0748	1.9048	5.68E-02	0.0325	0.0402	2.6341	1.8578
Temporal_Pole_Mid_R	Temporal_Sup_R	−5.1966	2.03E-07	0.0593	0.0443	−1.4504	1.47E-01	0.0262	0.0272	2.2682	1.6280
Temporal_Pole_Mid_R	Fusiform_R	−4.8828	1.05E-06	0.0427	0.0347	0.5730	5.67E-01	0.0215	0.0242	1.9857	1.4370
Temporal_Pole_Mid_R	Calcarine_R	−4.8335	1.34E-06	0.0463	0.0306	2.4275	1.52E-02	0.0083	0.0128	5.5968	2.3925
Temporal_Pole_Mid_R	Occipital_Inf_R	−4.7653	1.89E-06	0.0563	0.0417	1.0171	3.09E-01	0.0104	0.0131	5.4233	3.1793
Temporal_Pole_Mid_R	Frontal_Med_Orb_R	−4.7334	2.21E-06	0.0868	0.0706	−0.2756	7.83E-01	0.0211	0.0233	4.1105	3.0305
Temporal_Sup_L	Lingual_L	−4.6948	2.67E-06	0.0496	0.0419	−2.0835	3.72E-02	0.0293	0.0283	1.6914	1.4811
Temporal_Sup_L	Cuneus_L	−4.6358	3.55E-06	0.0448	0.0337	−1.5585	1.19E-01	0.0171	0.0154	2.6275	2.1915
Temporal_Sup_L	Occipital_Sup_L	−4.5831	4.58E-06	0.0364	0.0287	0.7577	4.49E-01	0.0165	0.0190	2.2047	1.5093
Thalamus_L	Thalamus_R	−5.7941	6.87E-09	0.0771	0.0651	−4.9874	6.12E-07	0.0830	0.0732	1.0770	1.1248
Thalamus_R	Thalamus_L	−4.9874	6.12E-07	0.0830	0.0732	−5.7941	6.87E-09	0.0771	0.0651	1.0770	1.1248
Thalamus_R	ParaHippocampal_R	4.8102	1.51E-06	0.0115	0.0199	3.0187	2.54E-03	0.0308	0.0392	2.6860	1.9657

Links are shown if their EC value in either direction exceeds the threshold of 0.03, and if there is a significant difference ($P < 0.05$) using FDR correction for multiple comparisons between patients and controls, for which the uncorrected significance level must be $P < 0.0012$. A negative value for z indicates a weaker effective connectivity link in patients with schizophrenia. Here we only show the top 80 links.

Table 2 Summary of the main differences in EC in schizophrenia

Region 1	Region 2 (a set of regions)	z value of region 1 to 2 EC	z value of region 2 to 1 EC	EC of region 1 to 2 in HC	EC of region 1 to 2 in SCZ	EC of region 2 to 1 in HC	EC of region 2 to 1 in SCZ
Precuneus_L	Hippocampus_L, ParaHippocampal_L, Occipital_Mid_L, Fusiform_L, Parietal_Sup_L, Paracentral_Lobule_L, Temporal_Sup_R, Paracentral_Lobule_R, Fusiform_R, Occipital_Mid_R, Hippocampus_R	4.229	0.510	0.0074	0.0134	0.0406	0.0465
Precuneus_R	ParaHippocampal_L, Occipital_Mid_L, Fusiform_L, Parietal_Sup_L, Temporal_Sup_R, Parietal_Sup_R, Occipital_Mid_R, ParaHippocampal_R, Hippocampus_R, Frontal_Sup_2_R	4.325	0.638	0.0104	0.0170	0.0441	0.0511
Cingulate_Post_R	Temporal_Mid_L, Temporal_Pole_Mid_R, Temporal_Mid_R, ParaHippocampal_R	3.679	−0.298	0.0081	0.0132	0.0558	0.0582
ParaHippocampal_L	Calcarine_L, Cuneus_L, Lingual_L, Occipital_Sup_L, Occipital_Mid_L, Occipital_Inf_L, Parietal_Sup_L, Temporal_Mid_L	−4.273	1.146	0.0405	0.0311	0.0140	0.0167
ParaHippocampal_R	Temporal_Pole_Sup_R, Parietal_Sup_R, Fusiform_R, Occipital_Inf_R, Occipital_Mid_R, Occipital_Sup_R, Lingual_R, Cuneus_R, Calcarine_R, Insula_R, Rectus_R, Olfactory_R	−4.796	0.432	0.0534	0.0416	0.0183	0.0205
Temporal_Sup_L	Cuneus_L, Lingual_L, Occipital_Sup_L	−4.638	−0.961	0.0436	0.0348	0.0210	0.0209
Temporal_Pole_Mid_L	Olfactory_L, OFCpost_L, Calcarine_L, Lingual_L, Occipital_Sup_L, Occipital_Mid_L, Occipital_Inf_L, Fusiform_L, Temporal_Sup_L, Temporal_Pole_Sup_L, Temporal_Mid_L	−4.477	0.424	0.0476	0.0374	0.0190	0.0216
Temporal_Pole_Mid_R	Temporal_Mid_R, Temporal_Pole_Sup_R, Temporal_Sup_R, Fusiform_R, Occipital_Inf_R, Occipital_Mid_R, Occipital_Sup_R, Lingual_R, Cuneus_R, Calcarine_R, ParaHippocampal_R, OFCpost_R, OFCmed_R, Rectus_R, Frontal_Med_Orb_R, Olfactory_R	−4.185	0.422	0.0548	0.0441	0.0199	0.0225
Fusiform_L	Frontal_Inf_Orb_2_L, Cuneus_L, Lingual_L, Occipital_Sup_L, Occipital_Mid_L, Lingual_R, Cuneus_R, Calcarine_R	−4.201	0.862	0.0620	0.0549	0.0244	0.0280
Fusiform_R	Occipital_Sup_L, Precuneus_L, Occipital_Sup_R, Lingual_R, Cuneus_R	−2.382	0.433	0.0635	0.0613	0.0230	0.0247
Amygdala_L	OFCpost_L, Insula_L, Postcentral_L, SupraMarginal_L	−4.265	−0.758	0.0230	0.0176	0.0337	0.0352
Cingulate_Ant_R	Cingulate_Mid_L, Cingulate_Post_R, Cingulate_Mid_R	−3.871	−1.330	0.0596	0.0546	0.0414	0.0410
Frontal_Sup_Medial_R	Cingulate_Mid_L, Cingulate_Mid_R, Cingulate_Ant_R	−3.521	−1.146	0.0307	0.0264	0.0514	0.0533
Supp_Motor_Area_L	Rolandic_Oper_L, Insula_L, Cingulate_Mid_L, Postcentral_L, Putamen_R, Frontal_Inf_Oper_R, Precentral_R,	−4.167	0.399	0.0345	0.0285	0.0429	0.0491
Supp_Motor_Area_R	Cingulate_Mid_L, Postcentral_L, Putamen_R, Postcentral_R, Cingulate_Mid_R, Insula_R, Rolandic_Oper_R, Frontal_Inf_Tri_R, Frontal_Inf_Oper_R, Precentral_R	−4.518	0.385	0.0491	0.0424	0.0382	0.0430
Precentral_L	Rolandic_Oper_L, Supp_Motor_Area_L, Postcentral_L, Heschl_L,	−2.214	−1.754	0.0672	0.0664	0.0400	0.0417
Precentral_R	Supp_Motor_Area_L, Parietal_Inf_R, Occipital_Mid_R	1.590	−1.874	0.0517	0.0633	0.0258	0.0237
Postcentral_R	Occipital_Mid_R, Lingual_R, Supp_Motor_Area_R,	−1.308	−3.205	0.0382	0.0385	0.0355	0.0326
Paracentral_Lobule_L	Precentral_L, Cingulate_Mid_L, Occipital_Sup_L, Postcentral_L, Parietal_Sup_L, Postcentral_R, Precentral_R,	−5.094	0.422	0.0434	0.0347	0.0566	0.0661
Paracentral_Lobule_R	Cingulate_Mid_L, Postcentral_L, Parietal_Sup_L, Postcentral_R, Precentral_R	−4.230	0.590	0.0425	0.0354	0.0602	0.0711
Heschl_L	Precentral_L, Cingulate_Mid_L, Postcentral_L, SupraMarginal_L, Temporal_Sup_L, Temporal_Mid_L, Heschl_R	−4.344	−2.163	0.0401	0.0344	0.0530	0.0500
Heschl_R	Temporal_Mid_R, Temporal_Pole_Sup_R, Temporal_Sup_R	−4.051	−1.953	0.0360	0.0332	0.0571	0.0560
Pallidum_R	Thalamus_L, Thalamus_R, SupraMarginal_R, Insula_R, Frontal_Inf_Oper_R	−4.317	−1.920	0.0408	0.0342	0.0250	0.0234
Putamen_R	SupraMarginal_R, Cingulate_Mid_R, Insula_R, Frontal_Inf_Oper_R	−4.271	−2.662	0.0450	0.0397	0.0271	0.0239

A positive value for z indicates a higher EC in SCZ.

in this step by general linear models (Barnes et al. 2010; Di Martino et al. 2014). After obtaining the *t*-test results for each center, the Liptak–Stouffer *z*-score method (Liptak 1958), which has been described in detail in our previous studies (Cheng et al. 2015a, 2015b, 2016), was then used to combine the results from the individual datasets. We note that in DCM, a threshold value for the EC may be applied, to make it likely that only biologically relevant values are considered (Stephan et al. 2010). In the current investigation we considered only EC values greater than a threshold value of 0.03 for a similar reason, and note that this provides a way to limit the number of links considered to a tractable set. The conclusions for the links described here would not be affected if a different threshold was chosen. In particular, altering the threshold does not alter the significance of the links, but merely how many links are assessed for significance. With a threshold of 0.03, 196 links were significantly different between schizophrenics and controls ($P < 0.01$ FDR corrected). When a lower threshold of 0.02 was used, more links were found to be significantly different between schizophrenics and controls, but all of the 196 links reported here were still present, so the results reported are robust to different thresholds. In general, the additional links selected with a threshold of 0.02 were less significantly different between schizophrenics and controls, and are not considered further here.

Analysis in terms of forward versus backward connectivity

The connections between adjacent cortical areas in a sensory hierarchy can usually be classified as forward (from the sensory input) versus backward (from an upper region in the hierarchy to the preceding region) (Rolls 2016a). Forward connectivity is often characterized by connections from layer 2–3 pyramidal cells forwards to layers 4, and 2 and 3, of the next cortical area. Backprojections between adjacent cortical areas in a hierarchy typically arise from the deep layers of the cerebral cortex, mainly layer 5, and project back mainly to layer 1 of the preceding cortical area (Markov et al. 2013, 2014a, 2014b; Markov and Kennedy 2013; Rolls 2016a). Give the termination on the apical dendrites in layer 1, far from the cell bodies, the backprojections are likely to be weaker than the forward connections, with effects reducing the backprojecting efficacy including shunting on the dendrites produced by other inputs to pyramidal cells. It is also crucial for attention and memory recall that the top-down or backprojections are weaker than the forward connections, so that attentional biasing and memory recall does not dominate over bottom-up forward inputs (Rolls and Deco 2002; Fuster 2008; Rolls 2016a). In areas of the brain apart from sensory hierarchies there may also be similar asymmetries for systems level functional reasons, for example, that short-term memory processing in prefrontal cortical areas does not dominate perceptual processing in the temporal and parietal areas that utilize the prefrontal cortex for short-term memory (Goldman-Rakic 1996). Because this asymmetry of the strength of the connectivity between brain regions is so important functionally, and usually has an anatomical basis, we have designated some of the effective connectivities analyzed in this investigation as forward or backward based on the strengths in each direction, as well as information about the anatomy of the different brain areas being connected (Rolls 2016a). It is at the same time the case that the effective connectivities can change to some extent based on whether sensory inputs versus memory recall (for example) is being performed, but nevertheless the forward and backward connectivity difference between many brain areas is large (as shown in the Results), and the concept of forward versus backward connectivity is utilized in this paper as an interesting way to characterize the functional differences that may be different between the patients and the controls.

Clinical correlates

We also investigated whether the differences in EC between patients and controls were correlated with symptoms assessed by the PANSS and illness duration. We used the Liptak–Stouffer *z*-score method (Liptak 1958) to combine the data from the different neuroimaging sites for this analysis, for this provides a principled way to take into consideration possible differences in these measures between sites. Specifically, we calculated the partial correlation between the normalized effective connectivities and the clinical scores, with head motion, age, sex, and education as covariates so that they did not contribute to the correlation between the ECs and the clinical scores, in each individual center. Then we used the Liptak–Stouffer *z*-score method to combine the results from the individual datasets (Liptak 1958).

Classification of individuals as with schizophrenia or controls using the EC

To further test the connectivities as diagnostic features for schizophrenia, we applied a support vector machine (SVM) approach using the whole EC or FC matrix as a biomarker to test how well this could discriminate schizophrenia patients from the healthy controls. These SVM classifiers were implemented by using MATLAB's fitcsvm.m, fitPosterior.m, and predict.m functions. Specifically, the polynomial kernel was used in the SVM classifier. All parameters including regularization parameter C, the polynomial kernel function order and the loss function were determined by the default setting of MATLAB.

Results

Differences of EC between patients with schizophrenia and controls

Table 1 shows the top 80 links with the most significant differences in EC between patients with schizophrenia and controls. In order to focus on links with a reasonable strength of EC that is likely to be meaningful in value (Rolls *et al.* 2018) as well as significantly different in schizophrenia, links are shown if their EC value in either direction exceeds the threshold of 0.03, and if there is a significant difference between patients and controls using FDR correction (corrected $P < 0.01$) for multiple comparisons, for which the significance level must be $P < 0.0012$ (Benjamini and Hochberg 1995). Figure 1 shows similar information in diagrammatic form, and includes all links (196 links in total) that satisfy the two criteria just described. Figure 2A shows these links between AAL2 nodes on views of the brain. Figure 2B shows the main areas with on average increases or decreases in their EC directed to other areas (Fig. 2C) in schizophrenia. Together, Figures 1 and 2 and Table 1 show, for example, that the main area with increases in EC directed toward other brain areas is the precuneus (and to a lesser extent the right precentral gyrus). Areas with mainly decreases in FC directed to other brain regions in schizophrenia include the parahippocampal gyrus, temporal cortical areas, the anterior cingulate cortex, and medial prefrontal cortex (Fig. 2B).

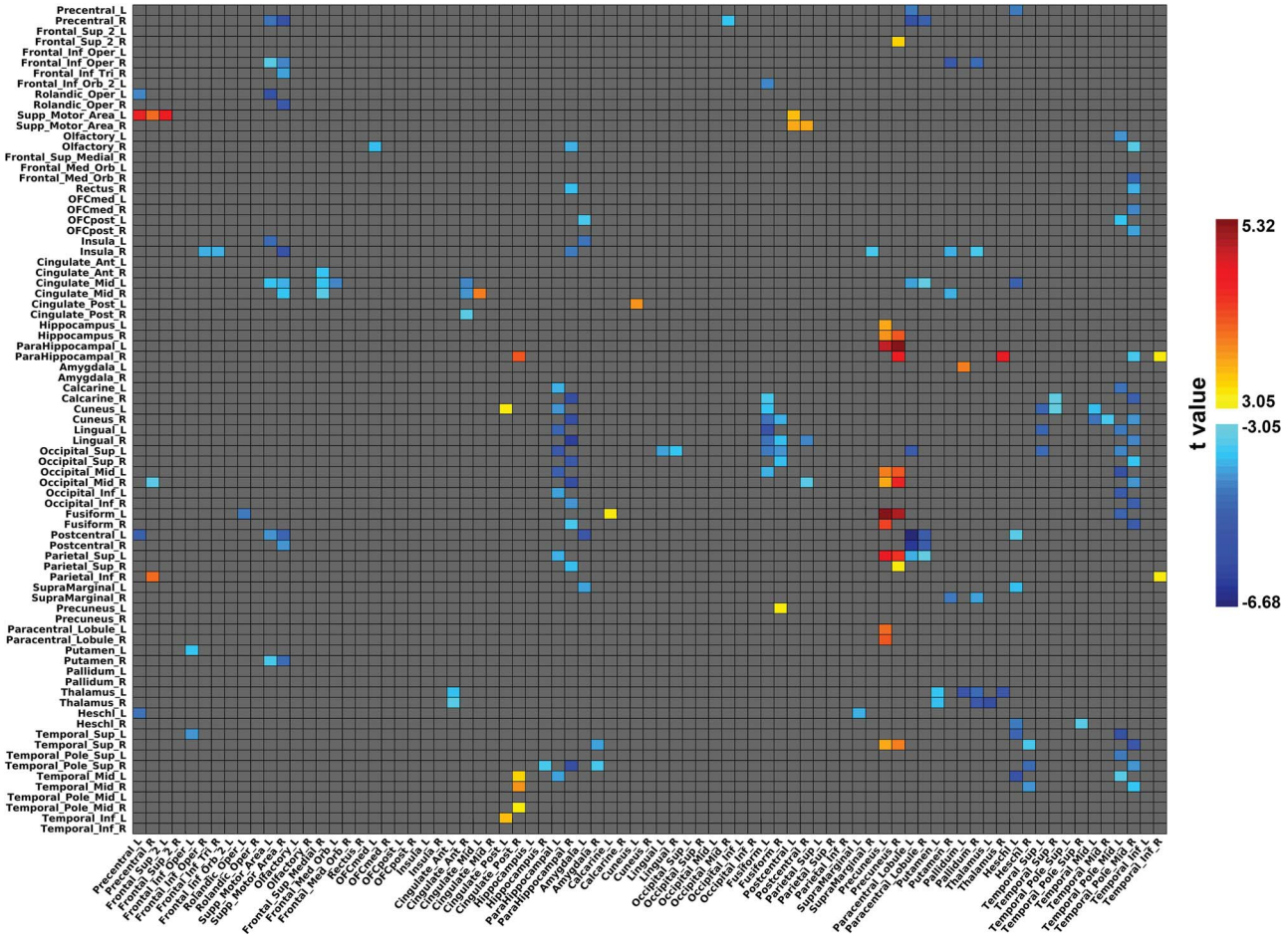

Figure 1. The matrices of differences in effective connectivity between schizophrenia patients and controls. The axes are the AAL2 areas, shown in their numbered order and with their names in Supplementary Table S1. The effective connectivity matrix has the index j for the columns and the index i for the rows. The matrix is thus non-symmetric, and the effective connectivity is always from j to i. The effective connectivity between any pair of links is shown in one direction in the upper right of the matrix, and in the opposite direction in the lower left.

Source regions of altered EC

Some of the quantitative changes in EC for the main regions are summarized in Tables 1–3, which show not only the statistically significant differences in EC in schizophrenia, but also the EC values in both directions in both the healthy controls and the patients with schizophrenia, as follows. Figure 1 complements this description. (Supplementary Tables S3 and S4 show the FC differences between the patients with schizophrenia and the healthy controls, for comparison).

First, the precuneus has high effective connectivities in schizophrenia directed to areas that include the parahippocampal and hippocampal cortices, temporal, fusiform and occipital areas, and superior parietal and paracentral cortices (Table 2). The direction of this increase of EC is the direction that is the weaker, which we refer to as a backprojection. The EC is almost not different between schizophrenics and controls in the forward direction.

Second, the EC from the closely related posterior cingulate cortex (PCC) to parahippocampal and temporal cortices is higher in schizophrenia (Table 2). The direction of this increase of EC is the direction that is the weaker, which we refer to as a backprojection. The EC is almost not different between schizophrenics and controls in the forward direction.

Third, the effective connectivities from the parahippocampal cortex to temporal, occipital, and calcarine mainly visual areas is lower in schizophrenia. This is the stronger direction of the connectivity. Some of these reduced effective connectivities were to medial orbitofrontal cortex areas (Rectus, OLF) and the insula.

Fourth, the EC from the temporal pole to medial orbitofrontal cortex areas (Rectus, OFCmed, OFCpost, Frontal_Med_Orb (ventromedial prefrontal cortex), OLF) were lower in schizophrenia. This is the stronger direction of the connectivity. The effective connectivities from temporal cortical areas to other temporal cortical areas and to occipital, calcarine, and lingual areas were also lower in schizophrenia.

Fifth, the fusiform gyrus (involved in face and other visual perception) has low EC in schizophrenia to the lateral orbitofrontal cortex (FrontalInfOrb2, involved in non-reward), to the precuneus and cuneus, and to early visual cortical areas. This is the stronger direction of the connectivity.

Sixth, the anterior cingulate cortex and the adjoining superior medial prefrontal cortex have low EC in schizophrenia to cingulate cortex regions.

Seventh, Heschl's gyrus (auditory) has low EC to temporal and some other areas.

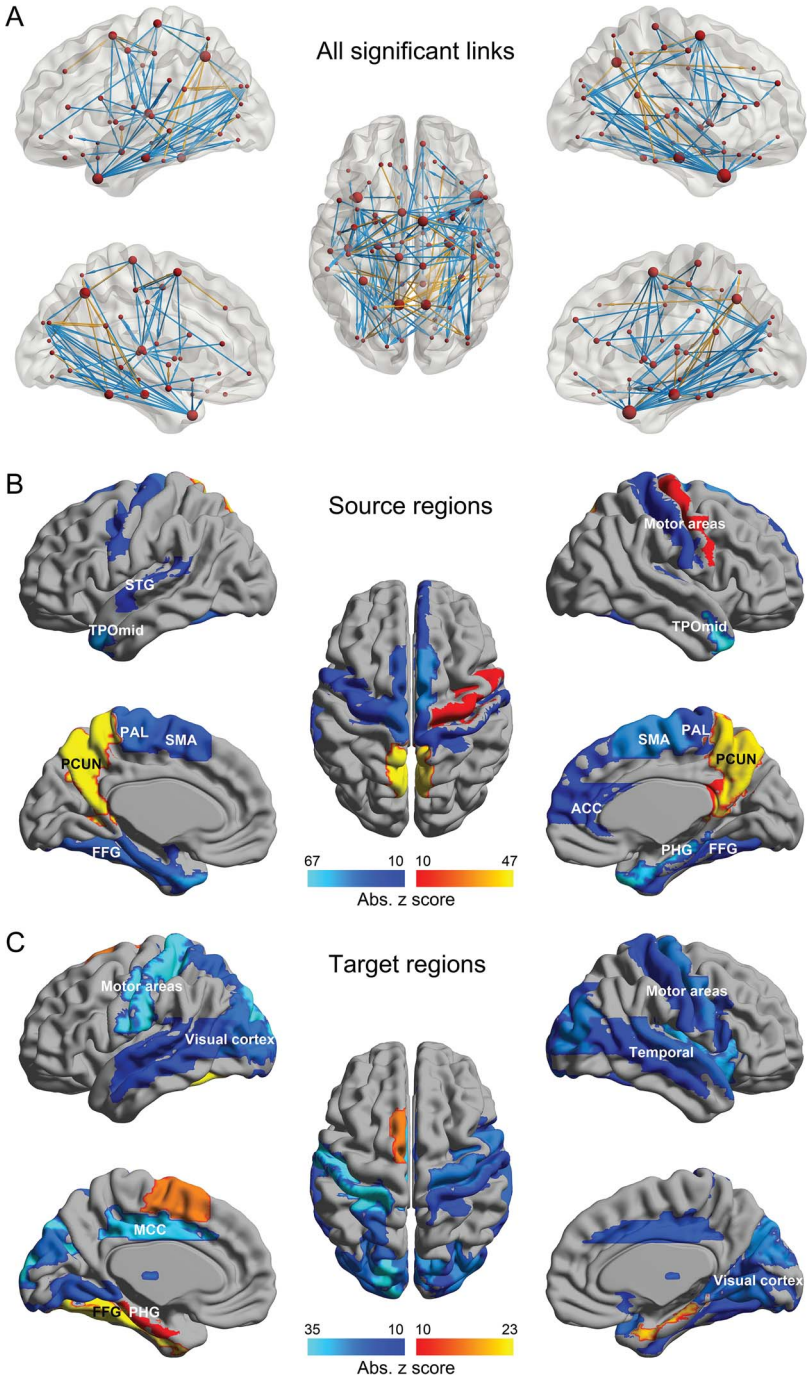

Figure 2. (*A*) Differences in effective connectivity between patients with schizophrenia and controls. The links shown are those with significantly different effective connectivity after FDR $P < 0.01$ correction. Yellow indicates that the effective connectivity is increased in patients, and blue that it is decreased. (*B*) The AAL2 atlas areas from which the effective connectivities were significantly different in patients with schizophrenia. (*C*) The AAL2 atlas areas to which the effective connectivities were significantly different in patients with schizophrenia. There were 196 such links in (*B*) and (*C*) significant with FDR correction, $P < 0.01$, and with effective connectivity values in at least one direction that were greater than 0.03.

Eighth, a number of motor/somatosensory regions (e.g., precentral, postcentral, paracentral, supplementary motor area) have low EC to other motor and other areas (Tables 1 and 2).

Target regions of altered EC

Tables 1 and 3 show areas that receive different EC from other areas in schizophrenia.

First, the parahippocampal gyrus receives increased EC in schizophrenia from temporal cortex areas (involved in perception), from the precuneus (involved in the sense of self), and from the posterior cingulate (involved in memory). This is the weaker direction of the connectivity.

Second, many temporal cortical areas and early visual cortical areas receive low EC in schizophrenia.

Table 3 Summary of the main differences in EC in schizophrenia

Region 1 (a set of regions)	Region 2	z value of region 1 to 2 EC	z value of region 2 to 1 EC	EC of region 1 to 2 in HC	EC of region 1 to 2 in SCZ	EC of region 2 to 1 in HC	EC of region 2 to 1 in SCZ
Cingulate_Post_L, ParaHippocampal_L, Fusiform_L, Temporal_Sup_L, Temporal_Mid_L, Temporal_Sup_R	Cuneus_L	−2.653	0.517	0.0414	0.0358	0.0179	0.0211
Fusiform_L, Temporal_Mid_L, Temporal_Pole_Mid_R, Temporal_Mid_R, Fusiform_R, ParaHippocampal_R	Cuneus_R	−4.315	0.713	0.0487	0.0398	0.0130	0.0147
Temporal_Inf_R, Temporal_Pole_Mid_R, Thalamus_R, Precuneus_R, Cingulate_Post_R	ParaHippocampal_R	2.720	−0.430	0.0215	0.0273	0.0478	0.0512
Frontal_Inf_Oper_L, Heschl_L, Temporal_Pole_Mid_L	Temporal_Sup_L	−4.789	−0.889	0.0460	0.0389	0.0430	0.0442
ParaHippocampal_L, Heschl_L, Temporal_Pole_Mid_L, Cingulate_Post_R	Temporal_Mid_L	−2.305	−0.799	0.0306	0.0287	0.0351	0.0367
Temporal_Pole_Mid_R, Heschl_R, Cingulate_Post_R	Temporal_Mid_R	−1.294	0.750	0.0342	0.0334	0.0413	0.0480
Temporal_Pole_Mid_R, Heschl_R, Amygdala_R, ParaHippocampal_R, Hippocampus_R	Temporal_Pole_Sup_R	−4.297	−0.292	0.0478	0.0421	0.0386	0.0408
Precuneus_L, Temporal_Pole_Mid_R, Heschl_R, Precuneus_R, Amygdala_R	Temporal_Sup_R	−0.990	−0.790	0.0286	0.0254	0.0427	0.0444
Rolandic_Oper_L, Calcarine_L, Precuneus_L, Temporal_Pole_Mid_L, Precuneus_R	Fusiform_L	0.960	0.286	0.0187	0.0192	0.0411	0.0457
Precuneus_L, Temporal_Pole_Mid_R, ParaHippocampal_R	Fusiform_R	−1.357	2.274	0.0350	0.0326	0.0305	0.0395
ParaHippocampal_L, Lingual_L, Fusiform_L, Paracentral_Lobule_L, Temporal_Sup_L, Temporal_Pole_Mid_L, Fusiform_R, Lingual_R	Occipital_Sup_L	−4.333	0.372	0.0468	0.0389	0.0253	0.0283
Temporal_Pole_Mid_R, Fusiform_R, ParaHippocampal_R	Occipital_Sup_R	−4.101	0.080	0.0468	0.0386	0.0170	0.0175
ParaHippocampal_L, Fusiform_L, Precuneus_L, Temporal_Pole_Mid_L, Precuneus_R	Occipital_Mid_L	−1.232	2.206	0.0289	0.0262	0.0274	0.0375
Precuneus_L, Temporal_Pole_Mid_R, Precuneus_R, Postcentral_R, ParaHippocampal_R, Precentral_R	Occipital_Mid_R	−1.393	0.133	0.0336	0.0307	0.0247	0.0292
ParaHippocampal_L, Fusiform_L, Temporal_Sup_L, Temporal_Pole_Mid_L	Lingual_L	−4.752	−0.426	0.0569	0.0474	0.0246	0.0258
Fusiform_L, Temporal_Pole_Mid_R, Postcentral_R, Fusiform_R, ParaHippocampal_R	Lingual_R	−4.555	−0.339	0.0657	0.0572	0.0227	0.0236
Fusiform_L, Temporal_Pole_Mid_R, Temporal_Sup_R, ParaHippocampal_R	Calcarine_R	−4.351	1.481	0.0475	0.0359	0.0145	0.0175
OFCmed_L, Temporal_Pole_Mid_R, ParaHippocampal_R	Olfactory_R	−3.650	−1.341	0.0544	0.0455	0.0260	0.0259
Supp_Motor_Area_L, Pallidum_R, Putamen_R, Supp_Motor_Area_R	Frontal_Inf_Oper_R	−4.316	−2.082	0.0419	0.0354	0.0319	0.0316
Pallidum_R, Putamen_R, SupraMarginal_R, ParaHippocampal_R, Supp_Motor_Area_R, Frontal_Inf_Tri_R, Frontal_Inf_Oper_R	Insula_R	−4.036	−1.671	0.0475	0.0420	0.0342	0.0331
Supp_Motor_Area_L, Frontal_Med_Orb_L, Paracentral_Lobule_L, Heschl_L, Paracentral_Lobule_R, Cingulate_Ant_R, Frontal_Sup_Medial_R, Supp_Motor_Area_R	Cingulate_Mid_L	−3.916	−0.002	0.0386	0.0327	0.0380	0.0418
Cingulate_Mid_L, Putamen_R, Cingulate_Ant_R, Frontal_Sup_Medial_R, Supp_Motor_Area_R	Cingulate_Mid_R	−2.181	−0.715	0.0442	0.0440	0.0580	0.0614
Precentral_L, Frontal_Sup_2_L, Postcentral_L, Precentral_R	Supp_Motor_Area_L	4.203	−2.269	0.0551	0.0740	0.0387	0.0379
Supp_Motor_Area_L, Paracentral_Lobule_L, Paracentral_Lobule_R, Occipital_Mid_R, Supp_Motor_Area_R	Precentral_R	−4.816	0.689	0.0439	0.0363	0.0704	0.0810
Paracentral_Lobule_L, Paracentral_Lobule_R, Supp_Motor_Area_R	Postcentral_R	−5.081	1.951	0.0521	0.0451	0.0554	0.0686
Precentral_L, Supp_Motor_Area_L, Amygdala_L, Paracentral_Lobule_L, Heschl_L, Paracentral_Lobule_R, Supp_Motor_Area_R	Postcentral_L	−4.830	1.545	0.0484	0.0410	0.0522	0.0619
ParaHippocampal_L, Precuneus_L, Paracentral_Lobule_L, Paracentral_Lobule_R, Precuneus_R	Parietal_Sup_L	−0.350	0.770	0.0336	0.0359	0.0336	0.0408
Cingulate_Ant_L, Putamen_L, Pallidum_L, Thalamus_R, Pallidum_R	Thalamus_L	−4.402	−1.482	0.0462	0.0398	0.0403	0.0404
Cingulate_Ant_L, Putamen_L, Thalamus_L, Pallidum_R	Thalamus_R	−4.476	−2.480	0.0433	0.0370	0.0465	0.0448

A positive value for z indicates a higher EC in SCZ.

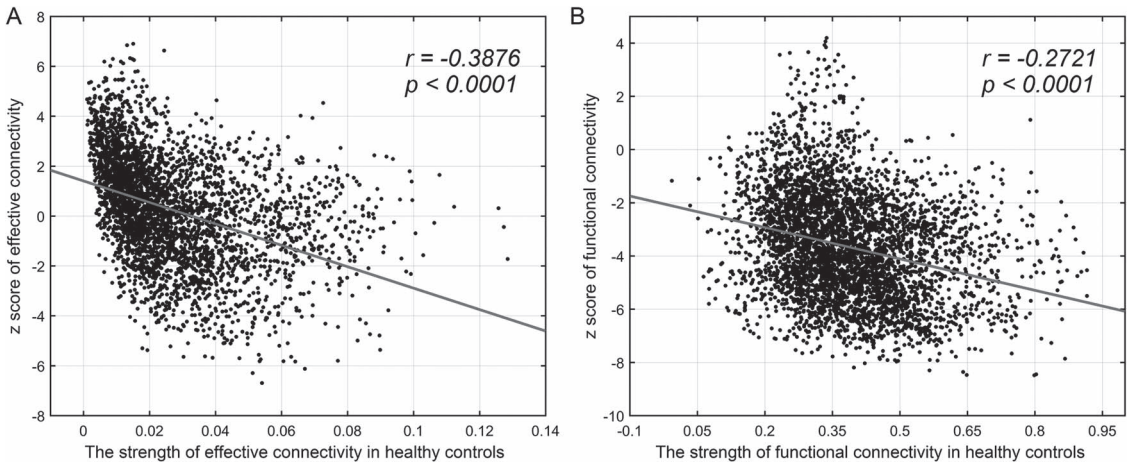

Figure 3. (*A*) The differences in effective connectivities (measured by the z score) in schizophrenia as a function of their strength in healthy controls. The links included are those that meet the two criteria used elsewhere, of a value for the EC > 0.03, and significantly different between patients and controls. (*B*) The differences in functional connectivities for the same links as in *A* in schizophrenia as a function of their strength in healthy controls. The links included are the same as those in *A*. Linear regression lines are shown for convenience, and provide evidence for a negative correlation between the difference in effective or FC in schizophrenia, and the strength of the effective connectivity.

Third, many motor and somatosensory areas receive low EC in schizophrenia.

Forward EC links tend to decrease in schizophrenia, and backward to increase in strength

Figure 3A makes the interesting point that strong effective connectivities tend to decrease in schizophrenia; and weak effective connectivities to increase in schizophrenia. Figure 3B makes a similar point for the functional connectivities in schizophrenia. This may be one prototypical rule for the changes in effective and FC in schizophrenia.

We hypothesized that what is shown in Figure 3A might be because in schizophrenia the stronger EC between any two areas, which normally conveys information forward from one cortical area to another from, for example, the sensory input up through a cortical hierarchy (Rolls 2016a), might tend to be reduced; and the weaker, "backward" or "top-down" effective connectivities might increase or show less difference in schizophrenia. To assess this, for each of the 196 links that had significantly different effective connectivities in schizophrenia, the forward versus backward direction was defined using the mean values from the whole group (controls and schizophrenics). (The forward direction was defined for the present analyses as the direction in which the EC was stronger.) Then the mean difference across participants between the value in the controls and the patients was calculated for each link. This was done separately for the forward and the backward link directions. A paired *t*-test was then performed of these differences across all 196 links. The *t* value for the forward links was −3.19, indicating that these links had lower values in the Forward direction in schizophrenia than in controls ($P = 0.0017$). The *t* value for the Backward links was 2.02 ($P = 0.045$), indicating that the mean of these links in the backward direction was higher in schizophrenia than in controls. The difference between the forward and backward effective connectivities was considerably smaller in the schizophrenia group than in the controls ($t = 3.77$, $P = 1.86e\text{-}4$).

In summary, these analyses provide evidence that for the effective connectivities that are significantly different in schizophrenia, the strength in the forward direction is smaller in schizophrenia, and in the backward direction is significantly higher in schizophrenia (as shown in Supplementary Fig. S2 and in the Supplementary material).

As a control to test whether these effects were specific for schizophrenia, the same analyses were performed in datasets of 338 individuals with major depressive disorder and 350 controls; and of 394 people with autism and 473 controls. The results are shown in Supplementary Figure S2 and show that for the significantly different effective connectivities in schizophrenia, on average the forward (stronger) effective connectivities were smaller, whereas the backward connectivities were little different or a little higher, in schizophrenia. The same selective lower forward EC was not found for the same links in separate populations with depression and with autism, suggesting that this pattern of smaller forward connectivity in schizophrenia for these links and relatively similar backprojections was characteristic of the population with schizophrenia. Details are provided in the Supplementary material.

Correlation between the effective connectivities and the schizophrenia symptom scores and the duration of the illness

The correlations between the mean PANSS scores for the positive, negative, and general symptoms, and for the total PANSS score (PANSS), and the illness duration, are shown in Table 4.

Most of the correlations were negative, indicating that weaker effective connectivities were associated with more severe symptoms. However, primarily for the precuneus, the correlations were positive, indicating that for the precuneus increased EC was associated with more severe symptoms.

For the precuneus, 11 of the EC links were correlated with the positive symptom PANSS score, including links to the hippocampus, temporal and fusiform cortex, parietal cortex, and occipital cortex. Four of the precuneus links were associated with the negative score, and five (mostly to occipital areas) with the general PANSS score.

The low effective connectivities in schizophrenia from the fusiform gyrus were especially associated with illness dura-

Table 4 The correlations between effective connectivity and clinical variables

EC: region 1 to region 2		Clinical variable	*r* value	*P* value	EC: region 1 to region 2		Clinical variable	*r* value	*P* value
Amygdala_R	Temporal_Sup_R	Duration	−0.158	0.0346	Precuneus_R	Occipital_Mid_L	General score	0.284	**0.0001**
Cingulate_Ant_R	Cingulate_Mid_L	General score	−0.147	0.0478	Precuneus_R	Occipital_Mid_L	PANSS	0.299	**0.0000**
Cingulate_Ant_R	Cingulate_Post_R	General score	−0.180	0.0134	Precuneus_R	Fusiform_L	Positive score	0.147	0.0490
Cingulate_Ant_R	Cingulate_Post_R	PANSS	−0.186	0.0109	Precuneus_R	Parietal_Sup_L	Positive score	0.220	0.0029
Frontal_Med_Orb_L	Cingulate_Mid_L	Duration	−0.187	0.0118	Precuneus_R	Parietal_Sup_L	Duration	0.148	0.0478
Frontal_Sup_2_L	Supp_Motor_Area_L	Duration	0.167	0.0259	Precuneus_R	Temporal_Sup_R	Positive score	0.200	0.0073
Fusiform_L	Frontal_Inf_Orb_2_L	Positive score	−0.168	0.0243	Precuneus_R	Temporal_Sup_R	Negative score	0.165	0.0275
Fusiform_L	Frontal_Inf_Orb_2_L	Duration	−0.176	0.0184	Precuneus_R	Temporal_Sup_R	PANSS	0.209	0.0049
Fusiform_L	Occipital_Mid_L	Duration	−0.204	0.0060	Precuneus_R	Occipital_Mid_R	Positive score	0.277	**0.0002**
Fusiform_R	Occipital_Sup_R	Duration	−0.191	0.0097	Precuneus_R	Occipital_Mid_R	Negative score	0.220	0.0031
Fusiform_R	Cuneus_R	Duration	−0.165	0.0261	Precuneus_R	Occipital_Mid_R	General score	0.317	**0.0000**
Lingual_L	Occipital_Sup_L	Duration	−0.160	0.0299	Precuneus_R	Occipital_Mid_R	PANSS	0.360	**0.0000**
Occipital_Mid_R	Precentral_R	Positive score	−0.148	0.0480	Precuneus_R	Frontal_Sup_2_R	Positive score	0.144	0.0498
Paracentral_Lobule_L	Occipital_Sup_L	Duration	−0.162	0.0275	Supp_Motor_Area_R	Cingulate_Mid_L	Duration	−0.170	0.0217
Paracentral_Lobule_L	Postcentral_R	Duration	−0.148	0.0478	Supp_Motor_Area_R	Postcentral_L	Duration	−0.158	0.0345
ParaHippocampal_R	Parietal_Sup_R	Negative score	−0.157	0.0357	Supp_Motor_Area_R	Rolandic_Oper_R	Duration	−0.163	0.0295
ParaHippocampal_R	Occipital_Inf_R	General score	−0.165	0.0263	SupraMarginal_R	Insula_R	General score	−0.156	0.0365
ParaHippocampal_R	Occipital_Sup_R	Negative score	−0.146	0.0389	Temporal_Inf_R	Parietal_Inf_R	Positive score	0.222	0.0027
ParaHippocampal_R	Occipital_Sup_R	Duration	−0.230	0.0019	Temporal_Inf_R	Parietal_Inf_R	General score	0.160	0.0326
ParaHippocampal_R	Cuneus_R	Negative score	−0.174	0.0158	Temporal_Inf_R	Parietal_Inf_R	PANSS	0.193	0.0095
ParaHippocampal_R	Cuneus_R	Duration	−0.241	0.0011	Temporal_Pole_Mid_L	Calcarine_L	Duration	−0.182	0.0144
ParaHippocampal_R	Olfactory_R	Negative score	−0.240	0.0010	Temporal_Pole_Mid_L	Occipital_Mid_L	General score	−0.159	0.0335
ParaHippocampal_R	Olfactory_R	PANSS	−0.199	0.0069	Temporal_Pole_Mid_L	Occipital_Inf_L	General score	−0.183	0.0137
Postcentral_R	Lingual_R	Duration	−0.156	0.0376	Temporal_Pole_Mid_L	Occipital_Inf_L	PANSS	−0.166	0.0263
Precentral_R	Occipital_Mid_R	PANSS	−0.166	0.0256	Temporal_Pole_Mid_L	Occipital_Inf_L	Duration	−0.217	0.0034
Precuneus_L	Occipital_Mid_L	Positive score	0.223	0.0027	Temporal_Pole_Mid_L	Temporal_Mid_L	Duration	−0.211	0.0045
Precuneus_L	Occipital_Mid_L	General score	0.209	0.0039	Temporal_Pole_Mid_R	Temporal_Mid_R	Duration	−0.185	0.0128
Precuneus_L	Occipital_Mid_L	PANSS	0.246	0.0006	Temporal_Pole_Mid_R	Temporal_Sup_R	Duration	−0.188	0.0111
Precuneus_L	Occipital_Mid_L	Duration	0.148	0.0484	Temporal_Pole_Mid_R	Calcarine_R	Positive score	−0.179	0.0160
Precuneus_L	Fusiform_L	Positive score	0.227	0.0022	Temporal_Pole_Mid_R	Calcarine_R	Negative score	−0.163	0.0297
Precuneus_L	Parietal_Sup_L	Positive score	0.243	0.0010	Temporal_Pole_Mid_R	Calcarine_R	General score	−0.170	0.0229
Precuneus_L	Parietal_Sup_L	PANSS	0.148	0.0485	Temporal_Pole_Mid_R	Calcarine_R	PANSS	−0.214	0.0040
Precuneus_L	Temporal_Sup_R	Positive score	0.164	0.0284	Temporal_Pole_Mid_R	Calcarine_R	Duration	−0.235	0.0012
Precuneus_L	Fusiform_R	Positive score	0.188	0.0113	Temporal_Pole_Mid_R	OFCmed_R	General score	−0.161	0.0312
Precuneus_L	Occipital_Mid_R	Positive score	0.151	0.0432	Temporal_Pole_Mid_R	OFCmed_R	PANSS	−0.163	0.0275
Precuneus_L	Occipital_Mid_R	General score	0.179	0.0160	Temporal_Pole_Mid_R	Olfactory_R	Negative score	−0.184	0.0137
Precuneus_L	Occipital_Mid_R	PANSS	0.187	0.0115	Temporal_Pole_Mid_R	Olfactory_R	PANSS	−0.150	0.0446
Precuneus_L	Hippocampus_R	Positive score	0.192	0.0097	Temporal_Pole_Sup_R	Heschl_R	Negative score	−0.155	0.0343
Precuneus_R	Occipital_Mid_L	Positive score	0.237	0.0014	Thalamus_L	Thalamus_R	Duration	−0.223	0.0027
Precuneus_R	Occipital_Mid_L	Negative score	0.149	0.0456	Thalamus_R	Thalamus_L	Duration	−0.228	0.0021

PANSS—positive and negative symptom total score. Positive, Negative, and General are the PANSS subscores. Duration—illness duration. Bold font shows correlations that pass FDR correction $P < 0.05$.

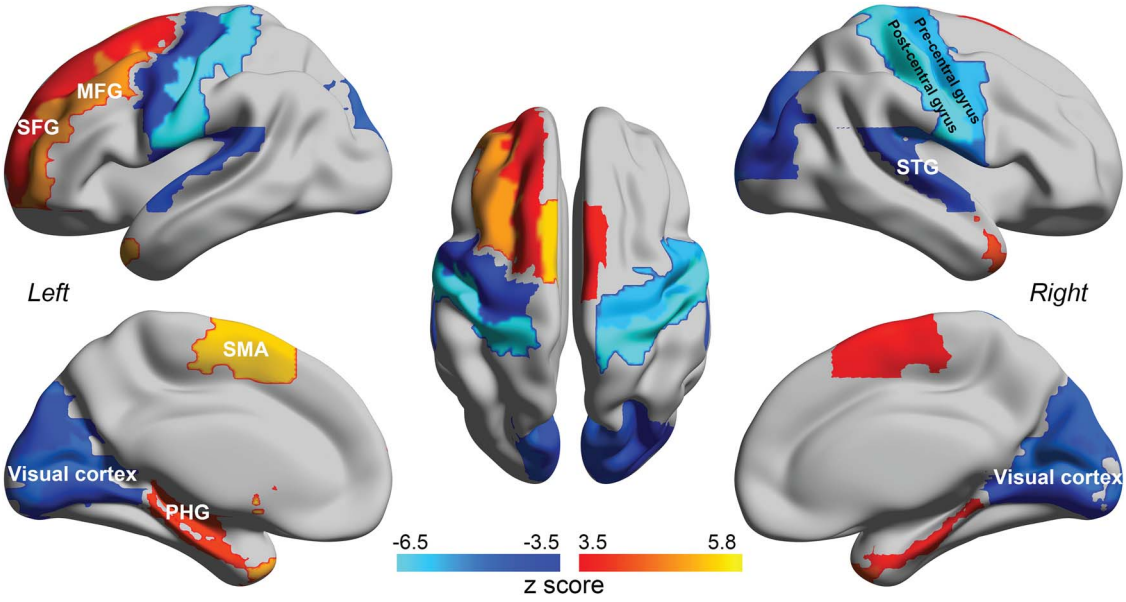

Figure 4. The results of the comparison of Σ between schizophrenia patients and healthy controls. This figure shows the AAL2 areas with significant differences after FDR correction ($P < 0.05$). Normalization of Σ was used across participants, applied in the same way as for the effective connectivity. Red–yellow indicates AAL2 regions with increased Σ, and blue with decreased Σ, in patients with schizophrenia (see Table 2).

tion. The low effective connectivities from the parahippocampal gyrus in schizophrenia were associated with the negative and general PANSS scores, and with illness duration. The low effective connectivities from the temporal cortical areas were especially associated with the negative and general PANSS symptoms and with illness duration.

In summary, the positive symptoms were especially likely to be associated with high effective connectivities from the precuneus; and the negative and general symptoms with low effective connectivities from areas such as the fusiform, temporal, and parahippocampal areas.

Differences in sigma in schizophrenia

Figure 4 and Table 5 show the differences in sigma in the population with schizophrenia.

Sigma is high in schizophrenia in areas such as the parahippocampal gyrus and hippocampus; the temporal pole; the superior frontal gyrus; the lateral orbitofrontal cortex; and the caudate nucleus and supplementary motor area. This is consistent with greater signal fluctuations in these regions. The result obtained with the approach used here is consistent with a previous finding that voxel-wise signal variance was increased in schizophrenia (Yang et al. 2014).

Sigma is low in schizophrenia in areas such as the cuneus, early visual cortical areas, Heschl's gyrus (auditory), and somatomotor areas such as the postcentral and precentral gyri.

Differences of FC between patients with schizophrenia and controls

For reference, we show in Supplementary Table S3 the top 80 links with the most significant differences in FC (measured by the Pearson correlation) between patients with schizophrenia and controls. Supplementary Table S4 shows the functional connectivities for the top 80 links with the most significant differences in EC between people with schizophrenia and controls. The first point of interest is that all the functional connectivities in these sets of links (apart from 1) were lower in schizophrenics than controls, whereas for the effective connectivities, higher effective connectivities were found for some precuneus and PCC effective connectivities (Supplementary Table S4). Second, there were 196 effective connectivities that were significantly different with FDR correction ($P < 0.01$) between schizophrenics and controls, whereas there were 3050 FC links that were significant with FDR ($P < 0.01$), and 1411 with Bonferroni correction ($P < 0.01$, see Fig. S1). The large number of significantly different functional connectivities in this analysis is of interest. We note that this is the first time that we have used unfiltered data for the functional connectivities. Third, prominent among the most different functional connectivities between schizophrenics and controls were links involving the inferior frontal gyrus and the motor cortex (Rolandic operculum).

These comparisons are of interest, for they elucidate one way in which effective connectivities can provide information that is not available from the functional connectivities.

Prediction of schizophrenia from the EC and FC

To further test the connectivities as diagnostic features of schizophrenia, we applied a SVM approach using the whole EC and FC as a biomarker to test how well this could discriminate schizophrenia patients from the healthy controls. We used a 10-fold cross-validation strategy to estimate the generalization of this classifier and to estimate its accuracy, sensitivity, and specificity. Table 6 shows that it is possible to predict (using an SVM) schizophrenia from the EC in the COBRE dataset from the Taiwan dataset and vice versa with a mean accuracy of 75.3%. This is a useful cross-validation. Table 6 also shows that this cross-validation prediction is a little better from the EC (75.3%) than from the FC (72.83%). Further, with the two datasets combined, the prediction of schizophrenia from the

Table 5 Σ values for AAL2 regions significantly different (FDR corrected) between schizophrenia patients and controls

Region	T value	P value	Region	T value	P value
Postcentral_R	−6.491	8.52E-11	Temporal_Pole_Mid_R	4.240	2.24E-05
Postcentral_L	−6.377	1.81E-10	Lingual_L	−4.199	2.69E-05
Precentral_R	−5.751	8.85E-09	Heschl_R	−4.107	4.00E-05
Caudate_L	5.735	9.77E-09	Hippocampus_L	4.087	4.37E-05
Caudate_R	5.667	1.46E-08	Cuneus_L	−4.084	4.43E-05
Supp_Motor_Area_L	5.329	9.86E-08	ParaHippocampal_L	4.051	5.11E-05
Temporal_Pole_Mid_L	5.066	4.07E-07	OFClat_L	4.013	6.01E-05
Rolandic_Oper_R	−5.052	4.38E-07	Temporal_Sup_R	−3.997	6.43E-05
Calcarine_R	−4.962	6.98E-07	Lingual_R	−3.861	1.13E-04
Frontal_Mid_L	4.871	1.11E-06	ParaHippocampal_R	3.850	1.18E-04
Calcarine_L	−4.833	1.34E-06	Occipital_Mid_R	−3.825	1.31E-04
Occipital_Sup_L	−4.804	1.55E-06	Supp_Motor_Area_R	3.772	1.62E-04
Cuneus_R	−4.635	3.57E-06	Frontal_Sup_L	3.723	1.97E-04
Occipital_Sup_R	−4.441	8.94E-06	Precentral_L	−3.657	2.55E-04
Temporal_Sup_L	−4.384	1.16E-05	Rolandic_Oper_L	−3.598	3.21E-04

A negative value for z indicates a lower sigma value in schizophrenia patients.

Table 6 The result of classification, that is, of which individuals have schizophrenia from the connectivities

Classification model	EC				FC			
	Accuracy	AUC	Sensitivity	Specificity	Accuracy	AUC	Sensitivity	Specificity
Taiwan only	87.32	95.12	86.03	88.49	81.09	89.13	78.11	83.78
COBRE only	79.86	88.81	76.72	82.39	75.22	84.46	69.69	79.67
Taiwan predict COBRE	76.15	82.61	67.24	83.33	71.53	78.18	65.52	76.39
COBRE predict Taiwan	74.52	80.35	75.61	73.53	74.13	82.19	73.17	75.00
All: Taiwan + COBRE	84.81	91.94	83.80	85.68	80.04	87.78	76.19	93.40

effective connectivities was 84.81%, and from the functional connectivities was 80.04% (Table 6). The importance of the EC links involving the precuneus is attested to by the results shown in Supplementary Table S5, which show that the prediction from the effective connectivities of who is schizophrenic is 69.02% correct based only on the precuneus effective connectivities.

Discussion

A key finding of this investigation in schizophrenia is the high EC directed away from the precuneus and the closely related PCC (Figs 1, 2, and 5 and Tables 1 and 2). The connectivity in the strong (or forward) direction in schizophrenia to the precuneus is similar to that in the healthy controls, and it is in the weak direction that the EC is higher in schizophrenia than in controls. An implication is that the normally weak backprojections from the precuneus to the areas that project to the precuneus are higher in schizophrenia than in controls. It is suggested that by influencing other areas too much by its backrojections, the precuneus may contribute to the symptoms of schizophrenia. The areas to which the backprojections from the precuneus are higher in schizophrenia than in controls include the parahippocampal and hippocampal cortices (Tables 1 and 2). The areas to which the backprojections from the PCC are higher in schizophrenia than in controls include the parahippocampal and temporal cortices (Tables 1 and 2).

We should therefore consider what the functions are of the precuneus and PCC. The precuneus is a medial parietal cortex region implicated in the sense of self, agency, autobiographical memory, and spatial function (Cavanna and Trimble 2006; Freton et al. 2014), and this may relate to the altered sense of self that is a feature of schizophrenia. The precuneus and the adjoining retrosplenial cortex (areas 29 and 30) (Kobayashi and Amaral 2000, 2003, 2007) (both included in the AAL2 area precuneus used here; Rolls *et al.* 2015) are key regions related to spatial function, memory, and navigation (Cavanna and Trimble 2006; Freton *et al.* 2014; Bubb et al. 2017). The retrosplenial cortex provides connections to and receives connections from the hippocampal system, connecting especially with the parahippocampal gyrus areas TF and TH, and with the subiculum (Kobayashi and Amaral 2003, 2007; Bubb *et al.* 2017). The precuneus can be conceptualized as providing access to the hippocampus for spatial and related information from the parietal cortex (given the rich connections between the precuneus and parietal cortex; Kobayashi and Amaral 2003, 2007; Vogt 2009). This increased EC from the precuneus to the hippocampal system is of special interest as it may contribute to the overactivity of the hippocampus in schizophrenia, which is consistent with the high sigma parameter in schizophrenia discussed below. Further, the precuneus has rich connectivity with the PCC (Vogt 2009), which provides a pathway into the hippocampal memory system (Rolls 2018; Rolls and Wirth 2018). The precuneus is part of the default mode network, which becomes more active when tasks are not being performed in the world, and instead internal thoughts and processing are occurring.

The PCC is also a key region of the default mode network with strong connectivity in primates with the entorhinal cortex and parahippocampal gyrus, and thus with the hippocampal memory system (Vogt and Pandya 1987; Vogt 2009; Bubb et al. 2017). The posterior cingulate region (including the retrosplenial cortex) is consistently engaged by a range of tasks that examine episodic memory including autobiographical memory,

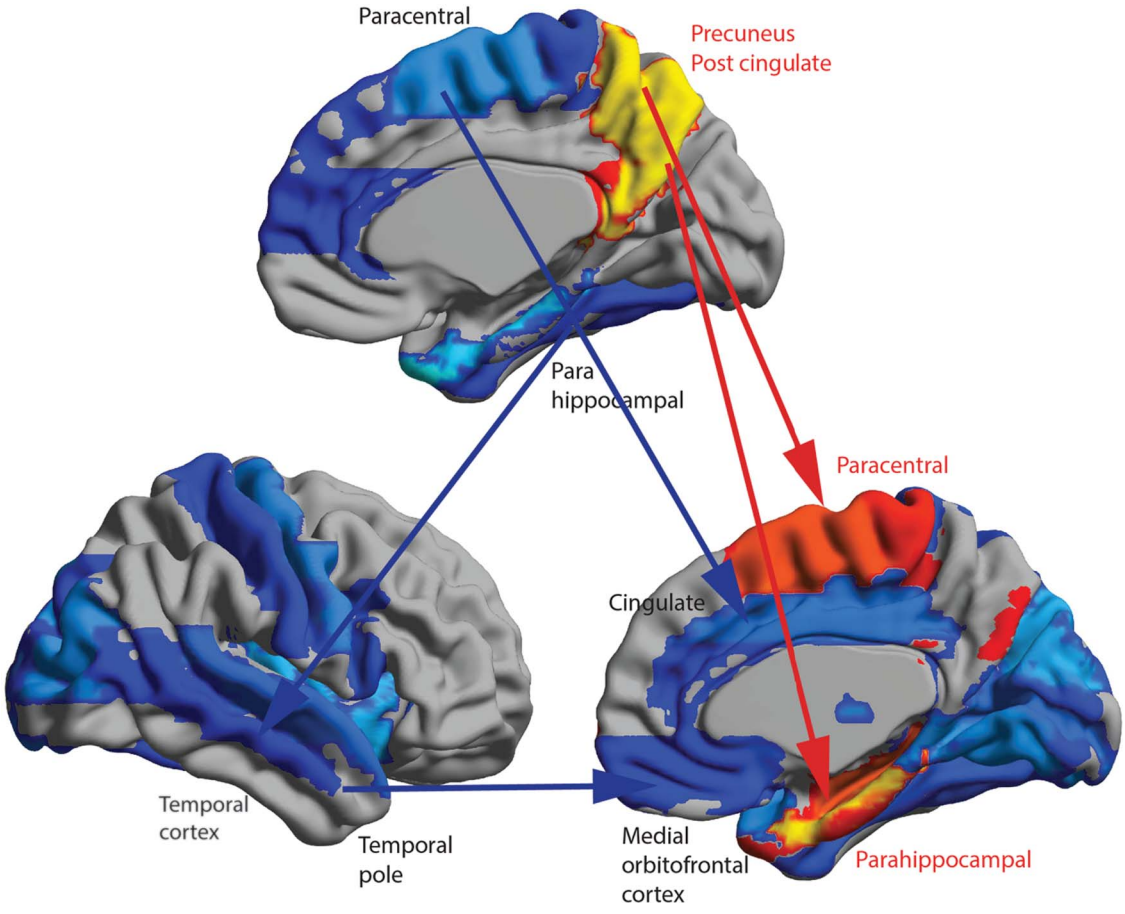

Figure 5. Summary of some of the main differences in effective connectivity in schizophrenia. The source regions (Region 1) are shown in the upper view of the brain, and the target regions (Region 2) in the two lower views of the brain. The AAL2 areas with these differences show higher effective connectivity in red to yellow; and lower effective connectivity in blue. The two main higher effective connectivities are shown here. Further lower effective connectivities were found than can be indicated in arrows, with the further details shown in Tables 1 and 4.

and imagining the future, and also spatial navigation and scene processing (Auger and Maguire 2013; Leech and Sharp 2014).

The proposal that we now make based on the findings described here and the evidence about the functions of the precuneus and PCC just considered is that the high backprojection effective connectivities from the precuneus may relate to increased internal thoughts about the self in schizophrenia, the world in which the self exists, and the relatively greater role of these internal thoughts that are not dominated by the sensory inputs from the word, which normally keep the self in contact with the real world and with real-word inputs. Correspondingly, we propose that the high backprojection effective connectivities from the PCC in schizophrenia may relate to increased memory-related internal thoughts involving relatively higher dominance of memories over the normal forward real-world sensory inputs that normally keep us in contact with the real world.

Consistent with this relative dominance of backprojection inputs from the precuneus and PCC over bottom-up sensory and related inputs from the real world, we found that most other effective connectivities that were different in schizophrenia involved low effective connectivities. These included low effective connectivities from Heschl's gyrus to temporal and some other areas, which might reduce the effects of external auditory input relative to internally generated auditory-related phenomena such as hearing internally generated voices. Perhaps correspondingly, the fusiform gyrus (involved in face and other visual perception; Kanwisher et al. 1997; Caspers et al. 2015) has low EC in schizophrenia to the lateral orbitofrontal cortex and to the precuneus and cuneus, which may reduce the impact of signals from the real world relative to internally generated scenarios. Thus, the proposal we make is that the reduced forward inputs to high-order areas such as the precuneus and PCC involved in the sense of self and of memories about the self, and the increased backward projections from the precuneus and PCC, lead to internally generated scenarios about the self becoming detached from and dominating the forward inputs normally brought to these regions from the real world.

Figure 3A makes the interesting point that strong effective connectivities tend to decrease in schizophrenia; and weak effective connectivities to increase in schizophrenia. Figure 3B makes a similar point for the functional connectivities in schizophrenia. In both cases, an important point is that there is a negative correlation between the difference in effective (or functional) connectivity in schizophrenia and the connectivity value. This may be one prototypical rule for the changes in effective and FC in schizophrenia. The decrease in the strong effective connectivities is consistent with the disconnection hypothesis (Friston and Frith 1995). An implication is that

the difference between the forward (defined as stronger) and backward (defined as weaker) EC between a pair of brain areas tends to be reduced in schizophrenia. As shown in the Results, across all links the forward connectivities (i.e., in the stronger direction) tended to be weaker in schizophrenia, with relatively little difference for the backward effective connectivities (those in the weaker direction). Moreover, this pattern was not found in the same way for the same EC links in two other mental disorders, depression and autism. An implication of this is that the feedforward sensory inputs from the world are less effective in schizophrenia; and that the top-down backward connectivities that mediate the effects of memory recall and attention (Rolls 2016a) show little difference in schizophrenia. This would tend to disconnect the individual from the world; and enclose the patient in an imaginary world too dominated by internal representations not corrected toward reality by sensory information from the world. Put in another way, if top-down signals are increased relative to bottom-up signals this would increase the importance of priors, that is, beliefs, at the cost of sensory signals, representing a possible mechanism for the emergence of hallucinations and delusions (Tschacher et al. 2017). In this sense, the present findings go beyond the disconnection hypothesis of schizophrenia (Friston and Frith 1995).

Another finding was of reduced effective connectivities between somatomotor and related areas (Tables 1, 2, and 3), and these may relate to the reduced sense of agency and being in control in schizophrenia.

Sigma was high in schizophrenia in the parahippocampal gyrus and hippocampus. This is consistent with greater signal (or signal fluctuations) in these regions. Consistent with this, hippocampal glutamate is increased in unmedicated schizophrenia, and a decrease of regional cerebral blood flow in the hippocampus produced by antipsychotics correlates with their efficacy (Birur et al. 2017). It is suggested that the reduced GluN1 receptor in the dentate gyrus may decrease pattern separation in the dentate (Das et al. 2014; Scott and Tamminga 2018), and lead to increased less sparse firing in CA3, which may make memories more similar to each other in schizophrenia, and promote a low memory capacity and frequent entries into the same few basins of attraction, corresponding to being confined to a space with a few over-stable memories. The high EC from the precuneus to the hippocampal system may contribute to the hippocampal overactivity in schizophrenia, we suggest.

The lateral orbitofrontal cortex, the temporal pole, and superior frontal gyrus also had a high sigma in schizophrenia. In the case of the temporal pole, it had reduced effective connective directed to a number of regions (Tables 2 and 3).

Sigma is low in schizophrenia in areas such as the cuneus, early visual cortical areas, Heschl's gyrus (auditory), and somatomotor areas such as the postcentral and precentral gyri. This is consistent with low-signal fluctuations in these regions in schizophrenia, and is also consistent with the hypothesis described above that there is reduced forward input from the world in schizophrenia, relative to the greater influence of top-down backprojections from areas such as the precuneus and PCC.

An important advantage of EC compared to FC in this investigation is that the EC measure shows that it is EC directed away from the precuneus and PCC that is increased in schizophrenia. An implication is that these are key regions that underlie schizophrenia. Moreover, as shown here, these normally weak backprojection effective connectivities from the precuneus are not only stronger in schizophrenia, but are correlated with the positive symptoms of schizophrenia. Another important advantage is that the measurement of EC enabled the discovery that the forward effective connectivities are reduced more than in the backward direction for the significantly different connections in schizophrenia (Fig. 5), which could not have been analyzed or understood with measures of FC, which reflect correlations and not directed effects between areas.

In the present investigation lower effective connectivities were found between many brain regions in schizophrenia (Tables 1–3; Figs 1–3). This is consistent with the hypothesis that one of the changes in schizophrenia is increased noise in these areas, due to reduced stability of cortical attractor networks in some brain regions (Loh et al. 2007a, 2007b; Rolls *et al.* 2008; Rolls and Deco 2011; Rolls 2012a).

The findings described here point toward two key potential advances in understanding the neurological basis of schizophrenia. First, increased EC from systems involving the precuneus, and PCC that are implicated in representations of the self, agency, and autobiographical memory may be a contributor to the often changed sense of self and agency in schizophrenia. Second, the generally reduced forward EC, but relatively similar backward EC, in schizophrenia compared to controls, may tend to result in over-emphasis on the internal world, with relative disconnection from the reality of the external world. This paper shows how taking EC into account can be very important in understanding the functions of the cerebral cortex, because it enables the forward and the backward connectivity between every pair of brain regions to be estimated. Having stronger forward than backward connectivity is crucial for the operation of many cortical systems, including systems for sensory processing, memory storage and recall, and top-down attention (Rolls 2016a), and the approach utilized here enables this issue to be investigated for a large number of different cortical and related areas. In this paper, we show how this may be important in understanding some mental disorders, such as schizophrenia.

Supplementary Material

Supplementary material is available at *Cerebral Cortex* online.

Funding

Shanghai Science and Technology Innovation Plan [No. 15JC1400101 and No. 16JC1420402 to J.F.], the National Natural Science Foundation of China [Grant No. 71661167002 and No. 91630314 to J. F.], The 111 Project [No.B18015 to J.F.], Shanghai Municipal Science and Technology Major Project [No.2018SHZDZX01 to J.F.] and ZJLab, National Natural Sciences Foundation of China [No.81701773, 11771010 to W.C.], Sponsored by Shanghai Sailing Program [No. 17YF1426200 to W.C.], Natural Science Foundation of Shanghai [No. 18ZR1404400 to W.C.], Ministry of Science and Technology, Taiwan [NSC100-2911-I-010-010, NSC101-2911-I-010-009, NSC100-2628-E-010-002-MY3, NSC102-2321-B-010-023, and NSC103-2911-I-010-501 to C.P.L.], National Health Research Institutes [NHRI-EX103-10310EI to C.P.L], Ministry of Health and Welfare of Taiwan (DOH102-TD-PB-111-NSC006 to C.P.L), Academia Sinica, Taipei, Taiwan [to C.P.L.], Human Brain Project (grant FP7-FET-ICT-604102 and H2020-720270 HBP SGA1 to G.D.) and the Marie Sklodowska-Curie Action (grant H2020-MSCA-656547 to M.G.).

Notes

Edmund T. Rolls, Wei Cheng and Jianfeng Feng contributed to the design of the study. Chun-Yi Zac Lo; Albert C. Yang; Shih-Jen Tsai; Mu-En Liu; Ching-Po Lin contributed to the collection of the data. Wei Cheng, Edmund T. Rolls, Matthieu Gilson, Gustavo Deco, and Weikang Gong contributed to the analysis of the data and the preparation of the manuscript. Edmund T. Rolls and Wei Cheng participated in writing the paper. All collaborators had an opportunity to contribute to the interpretation of the results and to the drafting of the manuscript. *Conflict of Interest*: None declared.

References

Auger SD, Maguire EA. 2013. Assessing the mechanism of response in the retrosplenial cortex of good and poor navigators. *Cortex*. 49:2904–2913.

Bajaj S, Adhikari BM, Friston KJ, Dhamala M. 2016. Bridging the gap: dynamic causal modeling and granger causality analysis of resting state functional magnetic resonance imaging. *Brain Connect*. 6:652–661.

Barnes J, Ridgway GR, Bartlett J, Henley SM, Lehmann M, Hobbs N, Clarkson MJ, MacManus DG, Ourselin S, Fox NC. 2010. Head size, age and gender adjustment in MRI studies: a necessary nuisance? *Neuroimage*. 53:1244–1255.

Benjamini Y, Hochberg Y. 1995. Controlling the false discovery rate: a practical and powerful approach to multiple testing. *J R Stat Soc Ser B Methodol*. 289–300.

Birur B, Kraguljac NV, Shelton RC, Lahti AC. 2017. Brain structure, function, and neurochemistry in schizophrenia and bipolar disorder-a systematic review of the magnetic resonance neuroimaging literature. *NPJ Schizophr*. 3:15.

Bubb EJ, Kinnavane L, Aggleton JP. 2017. Hippocampal—diencephalic—cingulate networks for memory and emotion: an anatomical guide. *Brain Neurosci Adv*. 1:1–20.

Caspers J, Palomero-Gallagher N, Caspers S, Schleicher A, Amunts K, Zilles K. 2015. Receptor architecture of visual areas in the face and word-form recognition region of the posterior fusiform gyrus. *Brain Struct Funct*. 220:205–219.

Cavanna AE, Trimble MR. 2006. The precuneus: a review of its functional anatomy and behavioural correlates. *Brain*. 129:564–583.

Cheng W, Palaniyappan L, Li M, Kendrick KM, Zhang J, Luo Q, Liu Z, Yu R, Deng W, Wang Q *et al*. 2015a. Voxel-based, brain-wide association study of aberrant functional connectivity in schizophrenia implicates thalamocortical circuitry. *NPJ Schizophr*. 1:15016.

Cheng W, Rolls ET, Gu H, Zhang J, Feng J. 2015b. Autism: reduced functional connectivity between cortical areas involved in face expression, theory of mind, and the sense of self. *Brain*. 138:1382–1393.

Cheng W, Rolls ET, Qiu J, Liu W, Tang Y, Huang CC, Wang X, Zhang J, Lin W, Zheng L *et al*. 2016. Medial reward and lateral non-reward orbitofrontal cortex circuits change in opposite directions in depression. *Brain*. 139:3296–3309.

Cox RW. 1996. AFNI: software for analysis and visualization of functional magnetic resonance neuroimages. *Comput Biomed Res*. 29:162–173.

Das T, Ivleva EI, Wagner AD, Stark CE, Tamminga CA. 2014. Loss of pattern separation performance in schizophrenia suggests dentate gyrus dysfunction. *Schizophr Res*. 159: 193–197.

Deco G, Kringelbach ML. 2014. Great expectations: using whole-brain computational connectomics for understanding neuropsychiatric disorders. *Neuron*. 84:892–905.

Di A, Yan CG, Li Q, Denio E, Castellanos FX, Alaerts K, Anderson JS, Assaf M, Bookheimer SY, Dapretto M *et al*. 2014. The autism brain imaging data exchange: towards a large-scale evaluation of the intrinsic brain architecture in autism. *Mol Psychiatry*. 19:659–667.

Frassle S, Lomakina EI, Razi A, Friston KJ, Buhmann JM, Stephan KE. 2017. Regression DCM for fMRI. *Neuroimage*. 155: 406–421.

Freton M, Lemogne C, Bergouignan L, Delaveau P, Lehericy S, Fossati P. 2014. The eye of the self: precuneus volume and visual perspective during autobiographical memory retrieval. *Brain Struct Funct*. 219:959–968.

Friston K. 2009. Causal modelling and brain connectivity in functional magnetic resonance imaging. *PLoS Biol*. 7:e33.

Friston K, Brown HR, Siemerkus J, Stephan KE. 2016. The dysconnection hypothesis (2016). *Schizophr Res*. 176:83–94.

Friston KJ. 2002. Bayesian estimation of dynamical systems: an application to fMRI. *Neuroimage*. 16:513–530.

Friston KJ, Frith CD. 1995. Schizophrenia: a disconnection syndrome? *Clin Neurosci*. 3:89–97.

Friston KJ, Kahan J, Biswal B, Razi A. 2014. A DCM for resting state fMRI. *Neuroimage*. 94:396–407.

Friston KJ, Mechelli A, Turner R, Price CJ. 2000. Nonlinear responses in fMRI: the balloon model, Volterra kernels, and other hemodynamics. *Neuroimage*. 12:466–477.

Fuster JM. 2008. *The prefrontal cortex*. London: Academic Press.

Gilson M. 2018. Analysis of fMRI data using noise-diffusion network models: a new covariance-coding perspective. *Biol Cybern*. 112:153–161.

Gilson M, Deco G, Friston KJ, Hagmann P, Mantini D, Betti V, Romani GL, Corbetta M. 2018. Effective connectivity inferred from fMRI transition dynamics during movie viewing points to a balanced reconfiguration of cortical interactions. *Neuroimage*. 180:534–546.

Gilson M, Moreno-Bote R, Ponce-Alvarez A, Ritter P, Deco G. 2016. Estimation of directed effective connectivity from fMRI functional connectivity hints at asymmetries in the cortical connectome. *PLoS Comput Biol*. 12:e1004762.

Goldman-Rakic PS. 1996. The prefrontal landscape: implications of functional architecture for understanding human mentation and the central executive. *Philos Trans R Soc B*. 351:1445–1453.

Greve DN, Fischl B. 2009. Accurate and robust brain image alignment using boundary-based registration. *Neuroimage*. 48:63–72.

Hagmann P, Cammoun L, Gigandet X, Meuli R, Honey CJ, Wedeen VJ, Sporns O. 2008. Mapping the structural core of human cerebral cortex. *PLoS Biol*. 6:e159.

Jenkinson M, Beckmann CF, Behrens TE, Woolrich MW, Smith SM. 2012. Fsl. *Neuroimage*. 62:782–790.

Kanwisher N, McDermott J, Chun MM. 1997. The fusiform face area: a module in human extrastriate cortex specialized for face perception. *J Neurosci*. 17:4302–4311.

Kay SR, Fiszbein A, Opler LA. 1987. The positive and negative syndrome scale (PANSS) for schizophrenia. *Schizophr Bull*. 13:261–276.

Khamsi R. 2012. Diagnosis by default. *Nat Med*. 18:338–340.

Kobayashi Y, Amaral DG. 2000. Macaque monkey retrosplenial cortex: I. three-dimensional and cytoarchitectonic organization. *J Comp Neurol*. 426:339–365.

Kobayashi Y, Amaral DG. 2003. Macaque monkey retrosplenial cortex: II. Cortical afferents. *J Comp Neurol*. 466: 48–79.

Kobayashi Y, Amaral DG. 2007. Macaque monkey retrosplenial cortex: III. Cortical efferents. *J Comp Neurol*. 502:810–833.

Leech R, Sharp DJ. 2014. The role of the posterior cingulate cortex in cognition and disease. *Brain*. 137:12–32.

Li T, Wang Q, Zhang J, Rolls ET, Yang W, Palaniyappan L, Zhang L, Cheng W, Yao Y, Liu Z *et al*. 2017. Brain-wide analysis of functional connectivity in first-episode and chronic stages of schizophrenia. *Schizophr Bull*. 43:436–448.

Liptak T. 1958. On the combination of independent tests. *Magyar Tud Akad Mat Kutato Int Kozl*. 3:171–197.

Loh M, Rolls ET, Deco G. 2007a. A dynamical systems hypothesis of schizophrenia. *PLoS Comput Biol*. 3:e228 doi:210.1371/journal.pcbi.0030228.

Loh M, Rolls ET, Deco G. 2007b. Statistical fluctuations in attractor networks related to schizophrenia. *Pharmacopsychiatry*. 40:S78–S84.

Markov NT, Ercsey-Ravasz M, Van Essen DC, Knoblauch K, Toroczkai Z, Kennedy H. 2013. Cortical high-density counterstream architectures. *Science*. 342:1238406.

Markov NT, Ercsey-Ravasz MM, Ribeiro Gomes AR, Lamy C, Magrou L, Vezoli J, Misery P, Falchier A, Quilodran R, Gariel MA *et al*. 2014a. A weighted and directed interareal connectivity matrix for macaque cerebral cortex. *Cereb Cortex*. 24:17–36.

Markov NT, Kennedy H. 2013. The importance of being hierarchical. *Curr Opin Neurobiol*. 23:187–194.

Markov NT, Vezoli J, Chameau P, Falchier A, Quilodran R, Huissoud C, Lamy C, Misery P, Giroud P, Ullman S *et al*. 2014b. Anatomy of hierarchy: feedforward and feedback pathways in macaque visual cortex. *J Comp Neurol*. 522:225–259.

Marreiros AC, Kiebel SJ, Friston KJ. 2008. Dynamic causal modelling for fMRI: a two-state model. *Neuroimage*. 39: 269–278.

Mayer AR, Ruhl D, Merideth F, Ling J, Hanlon FM, Bustillo J, Canive J. 2013. Functional imaging of the hemodynamic sensory gating response in schizophrenia. *Hum Brain Mapp*. 34: 2302–2312.

Messe A, Rudrauf D, Benali H, Marrelec G. 2014. Relating structure and function in the human brain: relative contributions of anatomy, stationary dynamics, and non-stationarities. *PLoS Comput Biol*. 10:e1003530.

Meyer-Lindenberg A. 2010. From maps to mechanisms through neuroimaging of schizophrenia. *Nature*. 468:194–202.

Mitra A, Snyder AZ, Tagliazucchi E, Laufs H, Raichle ME. 2015. Propagated infra-slow intrinsic brain activity reorganizes across wake and slow wave sleep. *Elife*. 4:e10781.

Mueser KT, McGurk SR. 2004. Schizophrenia. *Lancet*. 363:2063–2072.

Northoff G, Duncan NW. 2016. How do abnormalities in the brain's spontaneous activity translate into symptoms in schizophrenia? From an overview of resting state activity findings to a proposed spatiotemporal psychopathology. *Prog Neurobiol*. 145–146:26–45.

Pallares V, Insabato A, Sanjuan A, Kuhn S, Mantini D, Deco G, Gilson M. 2018. Extracting orthogonal subject- and condition-specific signatures from fMRI data using whole-brain effective connectivity. *Neuroimage*. 178:238–254.

Pandya DN, Seltzer B, Petrides M, Cipolloni PB. 2015. *Cerebral cortex: architecture, connections, and the dual origin concept*. New York: Oxford University Press.

Patel AX, Kundu P, Rubinov M, Jones PS, Vertes PE, Ersche KD, Suckling J, Bullmore ET. 2014. A wavelet method for modeling and despiking motion artifacts from resting-state fMRI time series. *Neuroimage*. 95: 287–304.

Razi A, Seghier ML, Zhou Y, McColgan P, Zeidman P, Park HJ, Sporns O, Rees G, Friston KJ. 2017. Large-scale DCMs for resting-state fMRI. *Netw Neurosci*. 1:222–241.

Rolls ET. 2012a. Glutamate, obsessive-compulsive disorder, schizophrenia, and the stability of cortical attractor neuronal networks. *Pharmacology, Biochemistry, and Behavior*. 100:736–751.

Rolls ET. 2012b. Invariant visual object and face recognition: neural and computational bases, and a model. *VisNet*. *Front Comput Neurosci*. 6(35):1–70.

Rolls ET. 2016a. *Cerebral cortex: principles of operation*. Oxford: Oxford University Press.

Rolls ET. 2016b. A non-reward attractor theory of depression. *Neurosci Biobehav Rev*. 68:47–58.

Rolls ET. 2018. The storage and recall of memories in the hippocampo-cortical system. *Cell Tissue Res*. 373:577–604.

Rolls ET. 2019. *The orbitofrontal cortex*. Oxford: Oxford University Press.

Rolls ET, Cheng W, Gilson M, Qiu J, Hu Z, Ruan H, Li Y, Huang CC, Yang AC, Tsai SJ *et al*. 2018. Effective connectivity in depression. *Biol Psychiatry Cogn Neurosci Neuroimaging*. 3: 187–197.

Rolls ET, Deco G. 2002. *Computational neuroscience of vision*. Oxford: Oxford University Press.

Rolls ET, Deco G. 2011. A computational neuroscience approach to schizophrenia and its onset. *Neurosci Biobehav Rev*. 35:1644–1653.

Rolls ET, Joliot M, Tzourio-Mazoyer N. 2015. Implementation of a new parcellation of the orbitofrontal cortex in the automated anatomical labeling atlas. *Neuroimage*. 122:1–5.

Rolls ET, Loh M, Deco G, Winterer G. 2008. Computational models of schizophrenia and dopamine modulation in the prefrontal cortex. *Nature Reviews Neuroscience*. 9: 696–709.

Rolls ET, Lu W, Wan L, Yan H, Wang C, Yang F, Tan Y-L, Li L, Chinese Schizophrenia Collaboration Group, Yan H *et al*. 2017. Individual differences in schizophrenia. *Br J Psych Open*. 3:1–8.

Rolls ET, Webb TJ, Deco G. 2012. Communication before coherence. *Eur J Neurosci*. 36:2689–2709.

Rolls ET, Wirth S. 2018. Spatial representations in the primate hippocampus, and their functions in memory and navigation. *Prog Neurobiol*. 171:90–113.

Scott D, Tamminga CA. 2018. Effects of genetic and environmental risk for schizophrenia on hippocampal activity and psychosis-like behavior in mice. *Behav Brain Res*. 339: 114–123.

Senden M, Reuter N, van den Heuvel MP, Goebel R, Deco G, Gilson M. 2018. Task-related effective connectivity reveals that the cortical rich club gates cortex-wide communication. *Hum Brain Mapp*. 39:1246–1262.

Smith K. 2012. Neuroscience: idle minds. *Nature*. 489:356–358.

Stephan KE, Penny WD, Moran RJ, den Ouden HE, Daunizeau J, Friston KJ. 2010. Ten simple rules for dynamic causal modeling. *Neuroimage*. 49:3099–3109.

Tschacher W, Giersch A, Friston K. 2017. Embodiment and schizophrenia: a review of implications and applications. *Schizophr Bull*. 43:745–753.

Valdes-Sosa PA, Roebroeck A, Daunizeau J, Friston K. 2011. Effective connectivity: influence, causality and biophysical modeling. *Neuroimage*. 58:339–361.

Vogt BA. 2009. *Cingulate neurobiology and disease*. Oxford: Oxford University Press.

Vogt BA, Pandya DN. 1987. Cingulate cortex of the rhesus monkey: II. Cortical afferents. *J Comp Neurol*. 262:271–289.

Whitfield-Gabrieli S, Ford JM. 2012. Default mode network activity and connectivity in psychopathology. *Annu Rev Clin Psychol*. 8:49–76.

Yang GJ, Murray JD, Repovs G, Cole MW, Savic A, Glasser MF, Pittenger C, Krystal JH, Wang XJ, Pearlson GD *et al*. 2014. Altered global brain signal in schizophrenia. *Proc Natl Acad Sci USA*. 111:7438–7443.